



# The influence of the ocean circulation state on ocean carbon storage and CO<sub>2</sub> drawdown potential in an Earth system model

Malin Ödalen<sup>1</sup>, Jonas Nycander<sup>1</sup>, Kevin I. C. Oliver<sup>2</sup>, Laurent Brodeau<sup>1,3</sup>, and Andy Ridgwell<sup>4,5</sup>

<sup>1</sup>Department of Meteorology, Stockholm University, 106 91 Stockholm, Sweden

<sup>2</sup>National Oceanography Centre, Southampton, University of Southampton, Southampton SO14 3ZH, United Kingdom

<sup>3</sup>Barcelona Supercomputer Center, Barcelona, Spain

<sup>4</sup>School of Geographical Sciences, Bristol University, Bristol, UK

<sup>5</sup>Department of Earth Sciences, University of California-Riverside, Riverside, CA, USA

*Correspondence to:* Malin Ödalen (malin.odalen@misu.su.se)

**Abstract.** During the four most recent glacial cycles, atmospheric CO<sub>2</sub> during glacial maxima has been lowered by about 90–100 ppm with respect to interglacials. There is widespread consensus that most of this carbon was partitioned in the ocean. It is however still debated which processes were dominant in achieving this increased carbon storage. In this paper, we use an Earth system model of intermediate complexity to constrain the range in ocean carbon storage for an ensemble of ocean circulation equilibrium states. We do a set of simulations where we run the model to pre-industrial equilibrium, but where we achieve different ocean circulation by changing forcing parameters such as wind stress, ocean diffusivity and atmospheric heat diffusivity. As a consequence, the ensemble members also have different ocean carbon reservoirs, global ocean average temperatures, biological pump efficiencies and conditions for air-sea CO<sub>2</sub> disequilibrium. We analyse changes in total ocean carbon storage and separate it into contributions by the solubility pump, the biological pump and the CO<sub>2</sub> disequilibrium component. We also relate these contributions to differences in strength of ocean overturning circulation. In cases with weaker circulation, we see that the ocean's capacity for carbon storage is larger. Depending on which ocean forcing parameter that is tuned, the origin of the change in carbon storage is different. When wind stress or ocean vertical diffusivity is changed, the response of the biological pump gives the most important effect on ocean carbon storage, whereas when atmospheric heat diffusivity or ocean horizontal diffusivity is changed, the solubility pump and the disequilibrium component are also important and sometimes dominant. Finally, we do a drawdown experiment, where we investigate the capacity for increased carbon storage by maximising the efficiency of the biological pump in our ensemble members. We conclude that different initial states for an ocean model result in different capacities for ocean carbon storage, due to differences in the ocean circulation state. This could explain why it is difficult to achieve comparable responses of the ocean carbon pumps in model intercomparison studies, where the initial states vary between models. The drawdown experiment highlights the importance of the strength of the biological pump in the control state for model studies of increased biological efficiency.

*Copyright statement.* All authors accept the licence and copyright agreement.



## 1 Introduction

When going from and interglacial toward a glacial maximum, atmospheric CO<sub>2</sub> is significantly lowered. During the last four glacial cycles (since  $\sim 400000$  years B.P.), the decrease has been about 1/3 and atmospheric  $pCO_2$  at these glacial maxima (marine isotope stages 2, 6, 8 and 10) was approximately 180 ppm (see e.g. Petit et al. (1999); Lüthi et al. (2008) and references therein). The ocean's capacity for storing carbon is many times larger than its atmospheric and terrestrial (biosphere) counterparts. CO<sub>2</sub> reacts with water to form bicarbonate and carbonate ions, and because of this, a lot more CO<sub>2</sub> than expected (compared to e.g. O<sub>2</sub>) is dissolved before chemical equilibrium is achieved. This leads to the ocean holding 50 times more carbon than the atmosphere (Williams and Follows, 2011; Falkowski et al., 2000) and over 13 times that of the terrestrial biosphere (Falkowski et al., 2000; IPCC, 2007). Due to this big difference in size between the carbon reservoirs, it is highly likely that most of the CO<sub>2</sub> that was taken out of the atmosphere during glacials was partitioned in the deep ocean rather than in the terrestrial biosphere (Kohfeld and Ridgwell, 2009).

That the oceanic carbon storage increased during glacials is a well established idea, and there are numerous studies of how and why this happened (e.g., Broecker, 1982; Sarmiento and Toggweiler, 1984; Archer et al., 2000a; Sigman and Boyle, 2000; Brovkin et al., 2007; Hain et al., 2010; Sigman et al., 2010). However, the relative effects of different processes contributing to this oceanic uptake have not yet been well constrained and, so far, there is a lack of consensus on which processes that were dominant (reviewed in Kohfeld and Ridgwell (2009)). Understanding these relative effects of oceanic CO<sub>2</sub> uptake mechanisms can also be important in other climate scenarios than glacial simulations.

To understand the oceanic uptake of CO<sub>2</sub> and the different processes involved, it is helpful to think about the different pathways that exist for carbon that is taken up in the surface layer to reach the deep ocean. These pathways are often referred to as the solubility pump and the biological pump (further described in Section 2.1). In this work, we focus on better constraining; 1) the effects of changes in global ocean mean temperature on the abiotic ocean-atmosphere CO<sub>2</sub> equilibrium and hence on the solubility pump; 2) the effect of changed CO<sub>2</sub> disequilibrium; and 3) the effects of increased efficiency of the biological pump. By performing ensemble runs using the Earth system model cGENIE (Ridgwell et al., 2007; Cao et al., 2009), we examine the changes in the carbon system that result from changes in ocean circulation.

Changes in ocean circulation, which can be due to climate change or other, independent physical processes (e.g. changes in bathymetry), will lead to changes in global ocean mean temperature, through e.g. redistribution and changes in formation rates of water masses. Firstly, if surface ocean temperature changes, this will have a direct effect on CO<sub>2</sub> solubility and hence on the atmosphere-ocean CO<sub>2</sub> equilibrium. Secondly, if the temperature, and thus the concentration of dissolved CO<sub>2</sub>, in the deepwater formation areas changes, this will impact on the deep-ocean concentration of CO<sub>2</sub> (Goodwin et al., 2011). Ocean circulation changes will also affect the ocean carbon content by influencing nutrient distributions, biological efficiency and time scales for outgassing of CO<sub>2</sub> in upwelling areas.

Model studies of glacial climate generally start from pre-industrial atmospheric CO<sub>2</sub>, that is prescribed, while the circulation model is tuned in order to achieve the target ocean fields of tracers such as salinity, temperature, and dissolved chemical compounds. However, the desired tracer fields can be achieved through multiple different combinations of the tuning parameters,



which means similar tracer fields can be achieved in different model states despite differences in their circulation. With this study, we aim to investigate the consequences of the circulation differences that result from this tuning; are there other aspects of the climate system, such as the strengths of the ocean carbon pumps, that become so significantly different that they can be crucial for the outcome of e.g. model intercomparison studies? As discussed in Zhang et al. (2013), overturning circulation differences in the initial glacial state can cause differences in results in model intercomparison studies of deglacial CO<sub>2</sub> rise.

Specifically, we aim to clarify how the ocean carbon storage, and in particular the CO<sub>2</sub> drawdown potential ( $DP$ , see Section 2.3, Eq. (3)), of a model depends on its equilibrium state. This will provide insight about why it is difficult to compare results from different model studies that have attempted to simulate and explain the lowering of atmospheric  $pCO_2$  (henceforth,  $pCO_2^{atm}$ ). One example of a model study where this dependence on the initial state may have been key is Archer et al. (2000b).

They investigated the abiotic chemical equilibrium in a few different models and showed that there was a consistent difference between box models and general circulation models (GCMs). They attributed this to differences in complexity. However, they also found a significant difference in behaviour between different GCMs, which they were unable to explain. We hypothesize, and show, that such differences could instead be due to differences in the initial state, where differences in circulation are causing the strengths of the carbon pumps, and thus model carbon inventories, to be different.

When studying glacial ocean CO<sub>2</sub> uptake, the most common modelling approach is to aim at reproducing a glacial climate by adjusting physical parameters, such as orbital parameters,  $pCO_2^{atm}$ , bathymetry, sea level, topography and/or ice sheets (e.g., Ganopolski et al., 2010; PMIP3), in ways that they may have changed during glacials. These, in turn influence the ocean circulation by affecting e.g. climate (temperature), tidal dissipation (Schmittner et al., 2015) and wind stress (Sime et al., 2013). In the first step of this modelling study, we instead do a process study where we change physical parameters in the model, one or two at a time, while restoring  $pCO_2^{atm}$  to the pre-industrial value. The parameters we change are common tuning parameters in climate models, such as wind stress intensity and ocean diffusivity. This approach allows us to see how the ocean circulation changes that follow from tuning each of these parameters affect the ocean carbon storage. We are particularly interested in the relative importance of the changes in the solubility pump, the biological pump and in CO<sub>2</sub> disequilibrium.

Through the first step of the modelling, we will show that the effect of changes in ocean circulation on global ocean mean temperature, and thus on the solubility pump, is significant and in some cases of similar importance as the effect on the biological pump. This first step will also allow us to discuss how specific changes to circulation parameters will influence the total carbon uptake in model simulations of e.g. glacial scenarios. In particular, we will focus on the influence of the strength of the global and basin scale overturning circulation.

In the second step, we enforce 100 % nutrient utilisation efficiency (see Section 2.3) in the different circulation patterns of the ensemble. This allows us to measure the difference in drawdown potential for CO<sub>2</sub> between different ocean circulation states. A new equilibrium in CO<sub>2</sub> between atmosphere and ocean will be established, and thus also  $pCO_2^{atm}$ , will be different depending on the ocean circulation. This will illustrate how the initial state of a model can be important for the outcome of a glacial CO<sub>2</sub> drawdown experiment and highlight the importance of differences in the initial states of models in intercomparison studies. Our theoretical approach is similar to those taken by Marinov et al. (2008a, b); Kwon et al. (2011). However, these studies all focus mainly on the contributions to ocean dissolved inorganic carbon ( $DIC$ ) by the biological pump. In this study,



we give equal attention to the perspective of the solubility pump and disequilibrium contributions to the total ocean carbon storage in a similar set of simulations.

Some general concepts and the framework we have used are introduced in Section 2. Theory and methods are described in Section 3. We then present the model ensemble output in Section 4. These results are discussed and put into perspective in  
5 Section 5.

## 2 Framework and general concepts

### 2.1 The carbon pumps

CO<sub>2</sub> that is dissolved in the ocean surface layer is often described as being able to reach the deep ocean via two pathways – the solubility pump and the biological pump. These pathways are thoroughly described in Volk and Hoffert (1985) and later  
10 in Williams and Follows (2011).

The abiotic (non-biological), physical pathway, or *the solubility pump*, begins with air-sea gas exchange, which acts to achieve a chemical equilibrium between the atmosphere and the surface ocean. This equilibrium depends on temperature. Colder surface water can dissolve more CO<sub>2</sub> which can then be transported (or pumped) down into the deep ocean with the  
15 ocean circulation. This carbon is also referred to as *preformed* carbon. Due to the fact that deep water forms in cold regions, the sinking water is enriched in carbon compared to surface waters in warmer regions. Since this cold water fills up the deep ocean everywhere, there will be a close link between the global ocean averages of temperature and preformed carbon.

The biological pathway, or *the biological pump*, begins with biological production in the surface ocean. Carbon is incorporated into soft-tissue organic compounds. Some of this material then reaches the deep ocean, either by being advected in currents or by simply falling out of the surface layer. When the organic material is decomposed, inorganic carbon (CO<sub>2</sub>) comes  
20 back into dissolution in the water. This fraction of DIC is referred to as *regenerated* carbon. Carbon is also incorporated into hard-tissue (shells) in the form of CaCO<sub>3</sub> which can be dissolved in the deep ocean. This dissolution influences deep ocean alkalinity (Section 2.2).

Due to the difference in the chemical role of soft-tissue and hard tissue carbon, the biological pump is more correctly referred to as being two separate pumps; the soft-tissue pump and the carbonate (hard-tissue) pump. The soft-tissue pump acts  
25 to increase deep ocean DIC, whereas the hard-tissue pump has a counter effect (Section 2.2), but net effect of the biological pump is to enhance the deep ocean concentration of DIC.

In the massive ocean carbon reservoir, about 90 % is expected to be preformed carbon and the remaining 10 % organic or regenerated carbon. (Williams and Follows, 2011). If the capacity of one or all of the carbon pumps to redistribute carbon from the surface to the deep ocean increased, this would act to decrease  $pCO_2^{atm}$ .



## 2.2 Alkalinity

An important player in the oceanic carbon cycle is alkalinity. It describes the buffer capacity of the ocean; hence, the ocean's capacity to resist a change in pH despite the addition of an acid, such as  $\text{CO}_2$ . Sea water total alkalinity is the number of moles of  $\text{H}^+$  equivalent to the excess of proton accepting ions (bases), mainly  $\text{CO}_3^{2-}$  and  $\text{HCO}_3^-$ , over proton donors (acids). If

5 there is an excess of proton acceptors, the addition of an acid to the sea water will only weakly affect the  $\text{pH}$  (Zeebe and Wolf-Gladrow, 2001). The main external source of alkalinity to the ocean is weathering of carbonates on land and the main sinks are precipitation of  $\text{CaCO}_3$  by marine organisms, such as microorganisms and reef building corals, and burial of these carbonates in both shallow and deep sea sediments (Sarmiento and Gruber, 2006).

Biological production affects the vertical distribution of ocean alkalinity, due to the hard-tissue pump. In the surface ocean, 10 some microorganisms such as coccolithophores and foraminifera surround their cells with a shell consisting of  $\text{CaCO}_3$ . Since  $\text{CO}_3^{2-}$  is one of the  $\text{H}^+$ -accepting ions that contribute to ocean alkalinity, the formation of shells will decrease the alkalinity of the surface ocean. This leads to a reduction of the surface ocean capacity to dissolve  $\text{CO}_2$ . Hence, this will act to increase  $\text{pCO}_2^{\text{atm}}$ . Due to this, the hard-tissue pump is sometimes called the 'carbonate counter pump' (Kohfeld and Ridgwell, 2009).

When the shells are exported to the deep ocean and dissolved, alkalinity is returned to solution. Hence, some of the alkalinity 15 in the deep ocean is of biological, or regenerated, origin. This part of the alkalinity, we will denote  $A_{\text{reg}}$ . The rest of the alkalinity in the deep ocean was set at the surface and then brought into the deep ocean by the circulation; this is preformed alkalinity,  $A_{\text{pre}}$ . Unlike  $\text{CO}_2$ ,  $A_{\text{pre}}$  does not have a typical, expected value, set by processes in the surface ocean. However, sea surface salinity and oxygen concentration are correlated with surface alkalinity and can therefore be used to estimate  $A_{\text{pre}}$  (see section 3.3).

20 Total alkalinity,  $A_T$ , is

$$A_T = A_{\text{pre}} + A_{\text{reg}} \quad (1)$$

This partitioning of alkalinity will be useful for understanding the relative importance of the hard-tissue biological pump in oceanic carbon storage.

It is likely that ocean alkalinity increased during glacials due to ice formation and associated sinking sea levels, causing e.g. 25 more weathering of carbonates. This may have contributed to the substantial drawdown of  $\text{CO}_2$  into the ocean that happened during glacials (see e.g. Sigman and Boyle (2000) and references therein).

In order to model the effect of alkalinity changes on  $\text{pCO}_2^{\text{atm}}$ , we would need an open ocean-atmosphere system with river supply and sedimentation of alkalinity. This would require a different type of modelling than we do here and our analysis is restricted to the ocean-atmosphere system, excluding sediment feedbacks.

## 30 2.3 Nutrient utilisation efficiency

Increased efficiency of the biological pump is a frequently proposed explanation for the glacial  $\text{CO}_2$  drawdown (eg. Sarmiento and Toggweiler (1984); Sigman and Boyle (2000)). By "increased efficiency" we mean that more of the available nutrients in



the surface layer are used for biological production before the water is subducted into the deep ocean. The remaining, unused, nutrients are brought with the circulation into the deep ocean, where no new production is possible. In the same way as carbon and alkalinity, the inorganic nutrients in the deep ocean can be separated into a preformed and a regenerated contribution; pre-formed nutrients are the unused nutrients subducted during deepwater formation (the physical pathway), whereas regenerated

5 nutrients have been transported to the deep via the biological pump (Ito and Follows, 2005).

When the nutrient utilisation efficiency is increased, the concentration of preformed nutrients,  $P_{pre}$ , decreases and the concentration of regenerated nutrients,  $P_{reg}$ , increases. This means that the biological pump gets stronger and transfers more carbon to the deep ocean. The air-sea equilibrium of  $\text{CO}_2$  is shifted and more  $\text{CO}_2$  is drawn from the atmosphere into the surface layer of the ocean, reducing  $p\text{CO}_2^{atm}$ .

10 As described in the framework introduced by Ito and Follows (2005), the global average of  $P_{reg}$  relative to the overall global average concentration of inorganic nutrients (denoted by  $P$ ) is a measure of nutrient utilisation efficiency. This can be described using the parameter  $\overline{P^*}$ ,

$$\overline{P^*} = \frac{\overline{P_{reg}}}{\overline{P}}. \quad (2)$$

15 Here, the overbars mark that we are using the global average of a quantity. If  $\overline{P^*}$  is 1, all available nutrients in the deep ocean were brought there by the biological pump. In other words, the deep ocean is ventilated by surface waters that have had all nutrients removed, hence (at steady state,) the ocean interior will have no preformed nutrients.

In Earth system models, how much  $\text{CO}_2$  that can be removed from the atmosphere by increasing the nutrient utilisation efficiency depends on  $\overline{P^*}$ , which can differ between models and between different climate states achieved in the same model (Marinov et al., 2008b). The difference between  $p\text{CO}_2^{atm}$  in the initial equilibrium state,  $p\text{CO}_2^{eq}$ , and the lowest  $p\text{CO}_2^{atm}$  that 20 can be achieved by increased nutrient utilisation efficiency,  $p\text{CO}_2^{min}$  (achieved when  $\overline{P^*} = 1$ ), will be referred to as the  $\text{CO}_2$  drawdown potential of a model,  $DP$ :

$$DP = p\text{CO}_2^{eq} - p\text{CO}_2^{min} \quad (3)$$

When the biological pump is working at maximum efficiency (when  $\overline{P^*} = 1$ ), we can assume that a specific amount of carbon proportional to the total amount of nutrients in the ocean will be trapped in the deep ocean at all times, assuming fixed 25 stoichiometric ratios (see Section 3.1.1). This carbon will not participate in the chemical equilibrium between atmosphere and ocean which decides the  $p\text{CO}_2^{atm}$ .



### 3 Methods

#### 3.1 Model

We use the model cGENIE, an Earth System Model of Intermediate Complexity (EMIC), which is a computationally efficient model developed for studying the ocean carbon cycle on timescales of  $\sim 100 - 100,000$  years. cGENIE is higher in complexity than box models, but is still efficient enough to allow running a large ensemble to equilibrium for the carbon system, and has a level of detail for the carbon system that made it particularly suitable for this study. Model characteristics are described in Edwards and Marsh (2005) and Ridgwell et al. (2007).

The physical ocean is modeled using a frictional-geostrophic 3D model on a 36x36 equal area grid in the horizontal and 16 depth levels. The atmospheric model is an Energy Moisture Balance Model (EMBM) with prescribed, climatological wind-fields. Ocean biogeochemistry and atmospheric chemistry are treated by separate modules that are coupled to the physical models and to each other. The biogeochemical module is based on a phosphate-only nutrient scheme. Hence, phosphate (P) is the limiting nutrient. The nitrogen (N) cycle is not modelled, but the effect of N on alkalinity during production and remineralisation of organic matter is represented. In those cases, N is assumed to have a fixed stoichiometric relationship with P (see Section 3.1.1).

As our control state, we use the pre-industrial equilibrium state described in Cao et al. (2009). During the spin-up (10,000 years) to this equilibrium state,  $pCO_2^{atm}$  is restored to 278  $\mu atm$  ( $\approx 278$  ppm), while the inventory of carbon in the model is allowed to change. Henceforth, this pre-industrial equilibrium state will be referred to as *PIES278*.

##### 3.1.1 Stoichiometry

The stoichimetric relationships in cGENIE is based on Redfield (1963). As such, there is, on average, a fixed relationship between the number of moles of the elements that are taken up (or released) in organic processes in the ocean. This relationship is  $N : P : C : O_2 = 16 : 1 : 106 : -138$ ; for each 1 mole of P used in biological production, 16 moles of N and 106 moles of C are also used, but 138 moles of  $O_2$  are released. The same relationship applies to the decomposition of organic material, which releases N, P and C, but consumes  $O_2$ . Any stoichiometric ratio involving oxygen is negative, e.g. the ratio between C and  $O_2$  is  $R_{C:O_2} = 106 / -138 \approx -0.768$ .

Adjustments to the stoichiometric ratios given in Redfield (1963) have been proposed by e.g. Takahashi et al. (1985) and Anderson and Sarmiento (1994), but the classic Redfield ratios are still widely accepted and used. The choice of constants is not crucial for the outcome of the study, and we have hence stayed with the default model setup of the official release of cGENIE.

More recently, the stoichiometry of production of new organic material has been shown to be highly variable, between species but also within the same species while living under different conditions, such as nutrient availability (e.g., Quere et al., 2005; Galbraith and Martiny, 2015). While this does not contradict that the ratios are on average similar to the results by Redfield (1963), this *in-situ* variability in stoichiometric ratios could potentially be important in a glacial scenario. However, evaluating the influence of such variability is beyond the scope of the present study.



### 3.1.2 Remineralisation scheme

Remineralisation in cGENIE primarily depends on oxygen availability, but if  $O_2$  is depleted and  $NO_3$  is selected as an active tracer, denitrification will allow for remineralisation to continue. When  $NO_3$  is depleted, sulphate reduction can also occur if  $SO_4^{2-}$  is an active tracer. When supply of oxidants is exhausted, remineralisation is inhibited.

5 In cGENIE, POC is modelled as two fractions: one more easily degradable (labile) fraction and one fraction that is more resistant to degradation. In terms of remineralisation, this means the labile fraction undergoes an exponential decay with depth, whereas the other fraction is remineralised at the ocean floor. The remineralisation scheme is described in detail in Ridgwell et al. (2007).

To further improve the representation of carbon fluxes to the deep ocean, a more explicit approach with several different 10 types of particulate organic matter with different reactivity can be used (Aumont et al., 2016).

## 3.2 Theory and experimental setup

The inventory of total carbon,  $TC$  [mol], in the equilibrium state can be described by

$$TC = M_a pCO_2^{atm} + M_o(\overline{C_{sat}} + \overline{C_{soft}} + \overline{C_{carb}} + \overline{C_{res}}) \quad (4)$$

Equation (4) sums the contributions to  $TC$ . The atmospheric carbon content, which in this model is limited to its content 15 of  $CO_2$ , is given by the partial pressure of  $CO_2$  times the number of moles of gas in the atmosphere,  $M_a$ . Assuming an atmospheric thickness of 7,777 m,  $M_a$  is given to  $1.7692 \cdot 10^{20}$  mol. In this case 1 ppm of  $CO_2$  corresponds to 2.123 PgC, which is consistent with the OCMIP recommendation.  $M_o$  is the mass of the ocean [kg], which in our ensemble of simulations is kept constant at  $1.34 \cdot 10^{21}$  kg. Implications of changes in volume are further discussed in Section 5.3. For one individual 20 water parcel,  $C_{sat}$  corresponds to the concentration [mol kg<sup>-1</sup>] of carbon the water parcel would have had if it would have been in equilibrium with the atmosphere, taking into account its temperature, salinity, alkalinity and also the minor effect of the concentration of  $PO_4$  in the absence of biology.  $C_{soft}$  corresponds to the carbon that has been added to the water parcel through the remineralisation of the soft tissue of biogenic material that has entered the water parcel. The biogenic material also carries hard tissue and the carbon contained in this tissue is denoted  $C_{carb}$ .  $C_{res}$  is the residual needed to get the actual carbon concentration in the water parcel.  $C_{res}$  contains three components; 1) The first, and most interesting, contribution to 25  $C_{res}$  is the disequilibrium component  $C_{dis}$ . This is the part of the water parcel carbon concentration which results from the water parcel not being in perfect equilibrium with the atmosphere at the time when it left the surface. Hence, the concentration of carbon of abiotic origin (preformed carbon) in the water parcel consists of  $C_{sat} + C_{dis}$ . 2) The second contribution to  $C_{res}$  is the presence of carbon in the form of particulate and dissolved organic matter. At any one model time step, the concentration 30 of such carbon is very small compared to the other terms in the equation ( $<1\%$ ,  $\sim 1 \cdot 10^{15}$  mol) and this is therefore not considered separately. 3) The third contribution to  $C_{res}$  consists of the errors associated with any imperfect assumptions in the theory used for calculating  $C_{sat}$ ,  $C_{soft}$  and  $C_{carb}$ . To allow us to distinguish between the components 1 and 3, we will make



simulations with artificially fast gas exchange to remove as much of  $C_{dis}$  as possible. These simulations are further described at the end of this section. The overbars represent global averages. In the deep ocean overall,  $C_{sat}$  and  $C_{res}$  together constitute the concentration of preformed carbon plus any calculation errors, whereas adding  $C_{soft}$  and  $C_{carb}$  gives regenerated carbon.

Initialising from our pre-industrial equilibrium state *PIES278*, we perform 12 different spin-ups in which one or two physical parameters have been changed compared to the control (Fig. 1, Table 1). They are run for 10,000 years, which is enough to reach a new equilibrium state. These sensitivity experiment equilibrium states are denoted *SE1 – SE12*. The physical parameters that we change are atmospheric heat diffusivity, wind stress and ocean vertical and horizontal diffusivity. They are selected because they are common tuning parameters (e.g., Müller et al., 2006; Marsh et al., 2013), which influence the ocean circulation.

These modifications of physical parameters will cause the ocean circulation to change c.f. *PIES278*; the circulation gets weaker/stronger, overturning cells change their latitudinal extent etc. During the spin-up phase,  $pCO_2^{atm}$  is still restored to 278 ppm (Fig. 1) and the ocean reservoir of nutrients (in this case,  $PO_4$ ) and alkalinity is the same as in *PIES278*. Hence, the atmospheric carbon inventory is identical in all ensemble members and in *PIES278*, but the ocean carbon inventory, as well as the  $TC$  of these 12 ensemble members will be different than in *PIES278*. We aim at comparing the drawdown potential of models that have the same  $pCO_2^{atm}$ , but different oceanic carbon distributions and inventories, which is usually the case in model intercomparison projects. For example, the instructions for the LGM simulations within the framework of the current PMIP3-CMIP5 project specify the LGM  $pCO_2^{atm}$  to be set to 185 ppm, whereas there are no specifications for the ocean carbon inventory (see <https://pmip3.lsce.ipsl.fr/>).

The change in the total carbon inventory,  $\Delta TC$  [mol] can be described by

$$20 \quad \Delta TC = M_o(\Delta \overline{C_{sat}} + \Delta \overline{C_{soft}} + \Delta \overline{C_{carb}} + \Delta \overline{C_{res}}) \quad (5)$$

The theoretically determined contributions by  $C_{soft}$ ,  $C_{carb}$  and  $C_{sat}$  to this observed change in  $TC$  in Eq. (5) are then evaluated as described in the subsections 3.3 and 3.4, excluding the change in  $C_{res}$ . The change in  $C_{res}$  will simply be the residual between the observed change in  $TC$  and sum of the theoretically determined contributions by  $C_{soft}$ ,  $C_{carb}$  and  $C_{sat}$ .

The changes in inventories of  $TC$ ,  $C_{sat}$ ,  $C_{soft}$ ,  $C_{carb}$  and  $C_{res}$  are translated into the equivalent change in  $pCO_2^{atm}$  that would occur if we were not restoring it to pre-industrial levels. This translation is performed as described in detail in Appendix A. This translation allows us to test the validity of the equation describing the effect on global ocean mean temperature effect on  $pCO_2^{atm}$  suggested by Goodwin et al. (2011) (see Appendix A)

Finally, starting from each of *SE1 – SE12* as well as from *PIES278*, we run experiments where the nutrient utilisation efficiency of biology is maximised (100 % efficiency) (Fig. 1) and again allow the model to run for 10,000 years to new equilibrium states (*DE1 – DE12*). This reveals the differences in drawdown potential between ensemble members with different ocean circulation characteristics. Maximum nutrient utilisation efficiency, i.e.  $\overline{P^*} = 1$  (see Eq. (2)), is achieved by changing the remineralisation length scale in the model. It is made deep enough (10,000 m) for any carbon that is taken up in organic material to be highly efficiently trapped in the deep ocean and not undergo any significant remineralisation. The concentration



of dissolved P (at the surface, and on a global annual mean) being reduced by two orders of magnitude in all *DE*:s, due to P being bound in organic material, confirms that this effect is achieved.

To calculate  $\overline{P}^*$  according to the framework by Ito and Follows (2005) (Section 2.3), we need to know  $\overline{P}_{reg}$ , the concentration of dissolved phosphate in the deep ocean that is of regenerated origin.  $\overline{P}_{reg}$  is derived from global average apparent oxygen utilisation,  $\overline{AOU}$ , using the Redfield ratio of phosphate to oxygen,  $R_{P:O_2}$ , as shown below in Eqs. 6-7. By removing  $\overline{P}_{reg}$  from the overall global average concentration of phosphate,  $\overline{P}$ , we get the global average concentration of preformed phosphate,  $\overline{P}_{pre}$  (see Eq. (8)).

$$\overline{P}_{reg} = -R_{P:O_2} \cdot \overline{AOU} \quad (6)$$

$$AOU = O_{2sat} - O_2 \quad (7)$$

$$10 \quad \overline{P}_{pre} = \overline{P} - \overline{P}_{reg} \quad (8)$$

As seen in Eq. (7),  $AOU$  is the difference between the saturation concentration of oxygen,  $O_{2sat}$ , which is the concentration that would be present if the water were at saturation at the ambient potential temperature and salinity, and the actual concentration of oxygen,  $O_2$ , that is registered in the water. It is assumed that most of this difference is due to decomposition of organic soft-tissue material, which consumes oxygen. According to Williams and Follows (2011), this is a valid assumption since the equilibration time with the atmosphere of oxygen at the ocean surface is only a few days. Hence, oxygen disequilibrium is likely to be small and  $O_2$  at the surface is very close to  $O_{2sat}$ . Therefore,  $AOU$  can be used to ‘back-track’ the amount of nutrients or carbon that was brought into the deep ocean trapped in organic material and which has then been remineralised.

The Ito and Follows framework has been widely applied, e.g. by Williams and Follows (2011); Marinov et al. (2008b); Kwon et al. (2011); Lauderdale et al. (2013). However, the validity of using this framework has been questioned (Bernardello et al., 2014). In the real ocean, oxygen disequilibrium is negative and though it is small, it is not negligible. The result is that  $P_{reg}$  and  $C_{soft}$  are overestimated when calculated with the ‘back-tracking’ method. This overestimation may not be critical when looking at the total global ocean inventory of carbon, but in the present study that looks at small changes in this inventory, the error is significant and of the same order of magnitude as the observed changes in  $C_{soft}$ . Hence, Bernardello et al. (2014) are right in their criticism. We have therefore made sure to eliminate this issue by running the model with artificially fast gas exchange for  $O_2$ , which rules out any disequilibrium effects on  $C_{soft}$ .

For  $CO_2$ , we have run the model with both fast and normal gas exchange, because we are interested in effects of  $C_{dis}$ . By applying fast gas exchange we are theoretically able to remove  $C_{dis}$  and can thus get an indication of how large the contributions of  $C_{dis}$  is to  $C_{res}$  in each simulation. To achieve artificially fast gas exchange we have multiplied the scaling constant ( $k = 0.31$ , following Wanninkhof (1992)) used in the calculation of the gas exchange coefficient by 100 (higher numbers did not achieve any significant difference) and removed the physical barrier effect of sea-ice on air-sea gas exchange.



### 3.3 Contribution by the biological pumps

The calculations in this section largely follow the Appendix in Lauderdale et al. (2013), who studied the correlation between wind-driven changes of the residual circulation in the Southern Ocean and changes in ocean carbon reservoirs and atmospheric CO<sub>2</sub>. All stoichiometric ratios for organic material are based on Redfield (1963) (see Section 3.1.1).

5 The ocean global average of  $C_{soft}$  is calculated from apparent oxygen utilisation,  $AOU$ , as

$$\overline{C_{soft}} = -R_{C:O_2} \cdot \overline{AOU}, \quad (9)$$

where  $R_{C:O_2}$  is the stoichiometric ratio of carbon to oxygen of  $-106/138 \approx -0.768$ . Here, we make use of the assumption that  $AOU$  is due to decomposition of organic soft-tissue material (see also Section 3.2).

10 To calculate the ocean inventory of  $C_{carb}$ , we need to know the preformed alkalinity,  $A_{pre}$ , of each grid cell. For this, we make a linear regression from model control state surface ocean data of salinity, oxygen and phosphate, similar to the regression made in Lauderdale et al. (2013). Note that the regression model is adapted for concentrations given in mmol L<sup>-1</sup> to be comparable to the regression made by Lauderdale et al. (2013).

$$A_{pre} = 0.0339 + 0.0642 \cdot S + 0.1777 \cdot PO \quad (10)$$

where

$$15 \quad PO = O_2 - R_{P:O_2} \cdot P. \quad (11)$$

Here,  $S$  is salinity and the second term represents the effect on alkalinity due to dilution. The third term represents alterations of alkalinity due to biological activity.  $PO$  is oxygen distribution with alterations due to respiration and remineralisation removed Broecker (1974),  $O_2$  is the oxygen concentration,  $P$  is the phosphate concentration and  $R_{P:O_2}$  is the stoichiometric ratio of phosphorus to oxygen of 1:138 ( $\approx -7.25 \cdot 10^{-3}$ ). This means that with a stronger biological pump, surface alkalinity 20 is reduced by a factor corresponding to this ratio.

We can now calculate the grid cell concentration of  $C_{carb}$  as

$$C_{carb} = \frac{1}{2} (A_T - A_{pre} - R_{N:O_2} \cdot AOU) \quad (12)$$

where  $A_{tot}$  is the grid cell alkalinity and  $R_{N:O_2}$  is the stoichiometric ratio of nitrogen to oxygen of 16:-138 ( $\approx -0.116$ ). We can then calculate the volume-weighted global average of  $C_{carb}$ .



### 3.4 Contribution by the solubility pump

Since  $pCO_2^{atm}$  is constant and the global ocean mean salinity is similar in all ensemble members  $SE1 - SE12$ , any changes in global average  $C_{sat}$  between  $PIES278$  and the  $SE$ :s will be due to changes in ocean temperature or alkalinity:

$$\overline{\Delta C_{sat}} = \overline{\Delta T \frac{\partial C_{sat}}{\partial T}} \Big|_{pCO_2, S, A_{pre}} + \overline{\Delta A_{pre} \frac{\partial C_{sat}}{\partial A_{pre}}} \Big|_{pCO_2, S, T} \quad (13)$$

5 Note: Salinity is conserved, but re-distributed. Hence, when using Eq. (13) at the local scale, the term dependent on  $\Delta S$  must be included. It only disappears after global integration, assuming that  $\frac{\partial C_{sat}}{\partial S} \simeq \text{constant}$ , which is done here.

We calculate the first term in Eq. (13) in a non-linear way, based on the changes in temperature in each grid cell of each ensemble member  $SE_n$  ( $n = 1 - 12$ ) compared to  $PIES278$ , while keeping salinity and alkalinity constant using the  $PIES278$  grid cell salinity and  $A_{pre}$ . We calculate the global average of grid cell  $C_{sat}(T_{SE_n}) - C_{sat}(T_{PIES278})$  solving the carbon 10 system equations using the solver CO2SYS (Lewis et al., 1998). The constants used in the scheme do not match exactly with those used in the model, but the differences are minor, which makes it relevant to assume that this is an acceptable choice.

The partial derivative in the second term on the right hand side of Eq. (13) is also calculated by solving the carbon system 15 equations using CO2SYS. While keeping  $T$  constant we change grid cell  $A_{pre}$  by 1 % to get  $\frac{\partial C_{sat}}{\partial A_{pre}}$ . To get the full contribution to  $\Delta C_{sat}$  by changes in  $A_{pre}$ , we then multiply by grid cell  $\Delta A_{pre}$  before averaging globally. Because the change in alkalinity is small between the different ensemble members, the contribution to the change in  $C_{sat}$  by the second term in Eq. (13) is much 20 smaller, and even negligible, compared to the contribution by changes in temperature (the first term).

In cGENIE, there is a restriction of the solubility coefficients for  $CO_2$  which are only defined for waters between 2–35 °C. Hence, all water below 2 °C has the same  $CO_2$  solubility in the model. In the calculations of  $C_{sat}$ , we use CO2SYS with this temperature limitation. The difference in global average  $C_{sat}$  between the case when this restriction is used with CO2SYS 25 compared to when it is not used is smaller than 0.6 % for all ensemble members, including the control state. Since the restriction is used consistently, the error caused by the restriction being present in the model should not constitute a significant problem for our analysis.

## 4 Results

We use a two-step modelling approach, as explained in Section 3.2; the first step is where we change the ocean circulation by 25 changing physical parameters as listed in Table 1, and the second is where we force the biology to become 100 % efficient. The results from this two-step approach is described in Sections 4.1 and 4.2.

### 4.1 Step 1 - The effects of ocean circulation changes

In this first step, we achieve a set of pre-industrial equilibrium states — all with pre-industrial  $pCO_2^{atm}$  of 278  $\mu\text{atm}$  — where, as a result of ocean circulation differences, the ensemble members have different carbon reservoirs. We use this set of 30 equilibrium states to investigate what controls these differences in reservoirs.



To allow for comparison between the control equilibrium state *PIES278* and the ensemble members *SE1* – *SE12*, Table 2 lists important diagnostic variables; global ocean averages of temperature ( $T_{avg}$ ) and pH ( $pH_{avg}$ ), surface ocean average pH ( $pH_{surf}$ ), global percentage of sea ice cover, global average nutrient utilisation efficiency (in terms of  $\bar{P}^*$ ) and a measure of the strength of the global ocean overturning circulation. For reference, the table also includes observational estimates (Locarnini et al., 2013; Comiso, 2008; Ito and Follows, 2005; Raven et al., 2005). In *PIES278* and *SE1* – *SE12*, global average salinity, alkalinity and  $PO_4$  are  $34.90$ ,  $2363 \mu mol kg^{-1}$  and  $2.15 \mu mol kg^{-1}$  respectively. These properties are conserved, but redistributed, which gives some very small differences in the global averages between ensemble members.

The changes in model total carbon inventory,  $\Delta TC$ , in the biological and the solubility pumps and the contributions from  $C_{res}$  (Eq. (5)) in the ensemble — which are effects of the changes in ocean circulation — are presented and compared in Fig. 10 2a. The control *PIES278* model  $TC$  inventory is  $3 \cdot 10^{18}$  mol ( $\sim 36,000$  Pg C), so the changes are of the magnitude of a few percent. This corresponds to a range in  $pH_{avg}$  between 7.79 and 7.97 (Table 2), while  $pH_{surf}$  stays close to the observational estimate ( $\sim 8.2$ , see Raven et al. (2005)).

For reference, we have also added a second panel (Fig. 2b), showing the changes in  $TC$  expressed as changes in  $pCO_2^{atm}$  (see Appendix A). Hence, if we were not restoring  $pCO_2^{atm}$  to pre-industrial conditions, but instead kept  $TC$  constant, this is 15 how much  $pCO_2^{atm}$  would approximately have changed due to the changes in physical characteristics of the system. In this ensemble, these changes in  $pCO_2^{atm}$  stay between  $\pm 50$  ppm.

The methods we use to convert our carbon inventory changes to changes in  $pCO_2^{atm}$  assume that the changes are small (Appendix A). Hence, the methods become less valid, and the estimates of the corresponding changes in  $CO_2$  become less reliable for ensemble members with greater changes, e.g. *SE4* and *SE12*. This should be kept in mind when examining 20 Fig. 2b. However, this is not considered a major issue, since these calculations are only made to give an idea of the order of magnitude of the effects on  $pCO_2^{atm}$  rather than exact numbers.

#### 4.1.1 Sensitivity of overturning streamfunction

In a coarse-resolution model like cGENIE, the overturning circulation, which transports carbon to the deep ocean and back up to the surface again (Eriksson and Welander, 1956), is one of the most sensitive circulation components.

25 The overturning circulation strength (henceforth denoted OVT) is diagnosed by taking the difference between the maximum and minimum (i.e. the maximum of the negative overturning cell) of the zonal average overturning streamfunction,  $\psi$ , below 556 m depth (excluding the uppermost five gridboxes).  $\psi$  for different ocean basins are shown in Table S.1.

Figure 3 suggests a linear relationship between the OVT and the total carbon inventory  $TC$ , in this case represented by  $\Delta TC$ , in the ensemble members. The relationship is clearer for the Atlantic and the global measure (Fig. 3a and 3c) than for 30 the Pacific (Fig. 3b). The correlation coefficients indicate that as much as 90 % of the variance in  $TC$  can be explained by changes in the OVT (Table 3).

For the different carbon pumps, the correlation with OVT is most clear for  $C_{soft}$  (see Fig. 4), where 73 – 79 % of the variance can be explained by the OVT (Table 3). Note that since no biogeochemical manipulations have been made in this step, the remaining variance (21 – 27 %) is also due to physical perturbations. For  $C_{sat}$  and  $C_{res}$ , the correlation is weak (26 – 49



% and 40 – 48 % respectively, Table 3), but statistically significant, especially for the Atlantic basin. If we add  $C_{soft}$  and  $C_{res}$  and correlate with the OVT, the correlation gets stronger than it is for  $C_{soft}$  alone.

In experiments with stronger OVT (global and basin scale) than in *PIES278*, e.g. *SE6* (see Figs. 5b, 2 and 8b), a water parcel will, on average, stay near the ocean surface for a shorter amount of time than if the OVT is weaker (e.g. *SE5*, see Figs. 5a, 2 and 8a). Hence, biology will have less time to use the nutrients available and  $\Delta C_{soft}$  will be negative. Meanwhile, there will be more mixing, leading to a deepening of the thermocline, and  $T_{avg}$  will increase. Thus,  $\Delta C_{sat}$  will also be negative. However,  $\Delta C_{res}$  will be more likely to be positive, due to changes in the temperature gradient (especially important in the North Atlantic), sea ice and outgassing (dominant in the Southern Ocean). These effects on  $C_{res}$  are further discussed in 4.1.5.

In experiments with stronger OVT (global and/or basin scale), the relative importance of  $\Delta C_{soft}$  (negative, see Table 3),  $\Delta C_{sat}$  (negative) and  $\Delta C_{res}$  (positive) will determine the sign of  $\Delta TC$ . In our ensemble, stronger OVT (global and basin scale) leads to a decreased storage of carbon in the ocean compared to *PIES278* (Figure 3).

Another important factor influencing the carbon pools is which overturning cell is dominating in terms of volume; the northern cell (producing North Atlantic Deepwater, NADW) or the southern cell (producing Antarctic Bottom Water, AABW, and Circumpolar Deep Water, CPDW). Since these water masses are of different origin, they will differ in properties, such as water temperature and nutrients, and will therefore have different capacities for holding  $C_{sat}$ ,  $C_{soft}$  and  $C_{res}$ . However, the inter-member differences in this aspect are difficult to discern and we have therefore chosen to focus on the impact of OVT described above, which are more clearly identifiable.

#### 4.1.2 Sensitivity of total carbon inventory

The relative contributions of the carbon pumps to  $\Delta TC$  are very different depending on the modified physical characteristics (Fig. 2). In experiments in which the modified atmospheric heat diffusivity is partly driving the circulation (and temperature) changes (*SE1*, *SE2* and *SE11*), the contributions by changes in the three components  $C_{soft}$ ,  $C_{sat}$  and  $C_{res}$  are of similar magnitude and are all important for the change in  $TC$ . This is also the case for some ensemble members with changes in ocean diffusivity (*SE7* and *SE9*).

In other experiments (e.g. with altered wind stress intensity, *SE*:s 3, 4 and 12) or in most cases where vertical diffusivity has been changed (*SE*:s 5, 6, 10)), the change in  $C_{soft}$  is dominant. In such experiments,  $\Delta C_{carb}$  can be as significant as  $\Delta C_{sat}$  and  $\Delta C_{res}$ , whereas it, in most other experiments, plays a minor role. In experiments where only the horizontal diffusivity has been changed (*SE*:a 7 and 8), the contributions by  $C_{sat}$  and  $C_{res}$  are larger than the contribution from  $C_{soft}$ .

This shows that no contributing terms can be considered negligible relative to the other terms. The importance of a given term for  $\Delta TC$  depends on the mechanism and the origin of the circulation change (Section 4.1.1).

In the following subsections, some results for each of the contributing terms are analysed.

#### 4.1.3 Sensitivity of biogenic carbon

Changes in  $C_{soft}$  and  $C_{carb}$  always have the same sign, but the effect of  $C_{carb}$  has a smaller magnitude (Fig. 2). The ratio  $\Delta C_{carb}/\Delta C_{soft}$  spans between 0.23 and 0.42 for *SE*:a 7 and 8 (halved and doubled horizontal ocean diffusivity respectively),



and spans 0.15 and 0.20 in other ensemble members. The effects that the changes in  $C_{soft}$  and  $C_{carb}$  have on  $pCO_2^{atm}$  are of opposite signs due to the effect of the carbonate pump on preformed alkalinity (Goodwin et al., 2008) (Fig. 2b).

Globally, about 75 % of the variance in  $C_{soft}$  is explained by the strength of the OVT (Fig. 4 and Table 3). This correlation is strongest over the Atlantic basin. The rest of the variance is likely explained by e.g. redistribution of nutrients, light limitation 5 regions or similar.

Fig. 6 b, suggests a tight, linear relationship between the inventory of  $C_{soft}$  and nutrient utilisation efficiency (here in terms of  $\bar{P}^*$ , Eq. (2)).  $P^*$  is a direct measure of the efficiency of the biological pump, and the linear relationship is expected from its definition (Eqs. 2, 6 and 7). Since the ratio between  $\Delta C_{carb}$  and  $\Delta C_{soft}$  is similar across ensemble members, the relationship between  $C_{carb}$  and  $\bar{P}^*$  is also fairly linear.

10 The relationship between  $TC$  and  $\bar{P}^*$  (Fig. 6 a) is quite linear too and is presumably dominated by  $C_{soft}$  and  $C_{carb}$  together (compare Figs. 6a and 6b). Deviations from a perfect straight line are caused by changes in the other carbon species. The influence of  $\Delta C_{sat}$  and  $\Delta C_{res}$  on  $\Delta TC$  can be fairly small compared to the influence of biogenic carbon (see Fig. 2, e.g. SE:s 3, 5, 6, 12) or fairly large but of opposite sign (see Fig. 2, e.g. SE:a 2, 4, 11), thus cancelling each other out to some extent, resulting in biogenic carbon “passing on” its linear relationship with  $\bar{P}^*$  to  $\Delta TC$ .

15  $\bar{P}^*$  is important for the drawdown potential of a model (Fig. 6c), which is examined in the second step of the modelling (Section 4.2).

#### 4.1.4 Sensitivity of temperature and saturation carbon

In the ensemble, global average temperature,  $T_{avg}$ , spans 2.3 and 4.9 °C, and in PIES278 it is 3.6 °C (see Table 2). This corresponds to an interval of change in ocean carbon storage of  $-1.4 \cdot 10^{16} - +1.3 \cdot 10^{16}$  mol (Fig. 2 a). Solving the carbon 20 system equations (Appendix A), indicates that this is equivalent to an interval of about -16 – +17 ppm in terms of  $pCO_2^{atm}$  change ( $\Delta pCO_2$ , Fig. 2 b.). The response in  $pCO_2^{atm}$  to changes in temperature is very close to linear; about 12.9 ppm °C<sup>-1</sup> (12.5–13.1 ppm °C<sup>-1</sup>, Fig. S1).

Calculating  $\Delta pCO_2$  for the temperature range of the ensemble using the simplified equation (A9) suggested by Goodwin et al. (2011), which is based directly on  $T_{avg}$  (Appendix A), gives an interval of -12 – +13 ppm. In this case, the linear fit gives 25 changes of 9.8 ppm °C<sup>-1</sup> (9.1–11.1 ppm °C<sup>-1</sup>, Fig. S1). For this ensemble, using the simplified equation yields results for  $\Delta pCO_2$  that in general differ by ~ 20–25 % compared to using the carbon system equation solver.

Fig. 2 stresses that the contribution by  $\Delta C_{sat}$  to  $\Delta TC$ , and hence to changes in  $pCO_2^{atm}$ , is nearly as important as the changes in  $C_{soft}$ . In ensemble members in which horizontal diffusivity in the ocean is changed,  $\Delta C_{sat}$  is larger than  $\Delta C_{soft}$ .

According to Headly and Severinghaus (2007), the global average temperature of the glacial ocean was  $2.6 \pm 0.6$  °C colder 30 than the modern day ocean. Since the ensemble member with the coldest ocean is only 1.3 °C colder than PIES278, the variations in  $C_{sat}$  during the past glacial cycles were likely larger than in our set of experiments.

The relationship between the changes in  $T_{avg}$  and  $\Delta C_{sat}$  is linear (Fig. 7), indicating that the changes in  $C_{sat}$  brought about by changes in alkalinity are insignificant in our model ensemble. The slope of the line is  $\frac{\partial C_{sat}}{\partial T} = -1.02 \cdot 10^{16}$  mol °C<sup>-1</sup>. If the global ocean cooled by ~ 2.6 °C, as expected in a glacial state, the slope of the line suggests the excursion in  $C_{sat}$  would be



$\sim 2.7 \cdot 10^{16}$  mol. In the context of a  $2.6^\circ\text{C}$  cooling, the carbon system equations (see Appendix A) yield that this corresponds to a decrease of about 30 ppm in  $pCO_2^{atm}$ . Here, we cannot use the simplified Eq. (A9), because the buffered carbon inventory is unknown in this hypothetical case.

The temperature sections in Fig. 8 show that when increased mixing is achieved by higher vertical diffusivity, this causes the 5 stratification to be less sharp between warm surface water and cold deepwater, because the warmer waters are mixed deeper. Thus,  $T_{avg}$  increases because of increasing vertical diffusivity. The colder, and more stratified simulation is also the simulation with the weakest OVT (Fig. 5a, Fig. 8a). Note: the deepest water in the Pacific Ocean is actually warmer in this simulation, but the effect of the shallower thermocline compensates for this and the net effect is a decreased  $T_{avg}$ . In the ensemble, simulations with a weaker OVT than PIES278 tend to have a lower  $T_{avg}$  and a larger ocean storage of  $TC$  (SE:s 1, 5, 8, 9 and 12 in 10 Table 2 and in Fig. 3). Despite this, the correlation between  $C_{sat}$  and the strength of the OVT (see Table 3) is weak. This is because the ocean cooling and the OVT are also influenced by other factors; as such they are not linearly related.

#### 4.1.5 Sensitivity of residual carbon

The global inventory of  $C_{res}$  in the initial equilibrium states is slightly negative in all cases and of the magnitude  $10^{16}$  mol (c.f. global  $TC$  inventory of  $\sim 3 \cdot 10^{18}$  mol). Hence, when we look at Fig. 2 and we see a positive contribution from  $C_{res}$ , keeping 15 in mind that the global inventories of  $C_{res}$  are negative in all ensemble members, this actually means it has only become less negative.

Comparing to observations described in Williams and Follows (2011), it seems like the inventory of  $C_{res}$  would be slightly positive or close to zero in the modern ocean (see the patterns in Fig. 11.21 and 11.22, where the Atlantic interior is slightly negative, but the surface and the Pacific are positive). Though Williams and Follows (2011) do not state a number for the global 20 inventory, they mention that the magnitude is close to the uncertainties in the analysis. Hence, it is possible, and even likely, that our global inventory of  $C_{res}$  is slightly negative due to these uncertainties.

When looking at  $C_{res}$ , we are mainly interested in the contribution by  $C_{dis}$ . The experiments with artificially fast gas exchange for  $\text{CO}_2$  indicate that the contribution to  $C_{res}$  by calculation errors (see Section 3.2) is in some cases of the same magnitude as the contribution by  $C_{dis}$ . This makes it difficult to constrain the effect of changes in  $C_{dis}$  in the ensemble by 25 looking at  $C_{res}$ . However, when the model is run with artificially fast gas exchange, noticeable changes in local DIC concentrations occur (examples shown in Fig. 9). These changes in DIC can be directly attributed to removing the contribution from  $C_{dis}$ . The changes are of the magnitude  $10\text{--}20 \mu\text{mol kg}^{-1}$ , which is on the order of 0.5–1 % of the grid cell DIC concentration. Hence, an ocean circulation change that drastically changes  $C_{dis}$  in the deep ocean will potentially see a significant contribution to  $\Delta TC$  from this component.

30 The processes influencing  $C_{dis}$  will be different in the deepwater formation areas in the Northern and Southern hemispheres (Toggweiler et al., 2003; Ito and Follows, 2005; Lauderdale et al., 2013). In the deepwater formation areas in the North Atlantic,  $C_{dis}$  is mainly a result of the temperature gradient. If a water parcel cools too fast before it sinks, there is not enough time to equilibrate with the atmosphere and the result will be a negative  $C_{dis}$ . This is seen as a negative signal in the upper half of the sections in Figure 9c. In a warmer global ocean, the temperature gradient between the equator and the poles will be



smaller. This makes it easier for a parcel travelling north in the Atlantic to reach equilibrium with the atmosphere before deepwater forms, since the parcel does not have to cool as much as in a colder simulation. In a warmer ocean, there is also less sea ice preventing exchange with the atmosphere. However, a warmer global ocean is often associated with faster circulation (see Section 4.1.1), and if the circulation becomes faster at the same time, the negative effect of the shorter time available for 5 equilibration will compete with the positive effect of a smaller temperature gradient and less sea ice. In some cases, but not all, the warmer high latitude temperatures can compensate for the speed up of the circulation.

In the Southern Ocean there will also be less time for the surface water to equilibrate its gas concentrations with the atmosphere. Here, oversaturated deepwater coming back to the surface in this area may not have the time to release its carbon to the atmosphere before the water sinks back into the deep, producing positive  $C_{dis}$ . This appears as a positive signal in the lower 10 half of the sections in Figure 9c. In a case with faster circulation, the contribution of positive  $C_{dis}$  will be even larger. This effect dominates over the temperature gradient effect in this area, because the waters being brought back to the surface are already very cold. However, in this model, the effect of sea ice on  $C_{dis}$  can also be very pronounced in this area, if it caps the upwelling area and prevents outgassing.

As we have seen in Figure 9, the local effects of  $C_{dis}$  for the simulations with artificially fast gas exchange are noticeable. 15 Despite this, the net effect on global ocean  $TC$  by the changes in  $C_{dis}$  is very small (on the order of 0.01 %). This is due to the fact that both the northern and the southern sinking are affected simultaneously; since they are of opposite signs they cancel each other. In a case with changes in ocean circulation, both sinking branches are not necessarily affected to equal amounts. As we will see below, this means the net effect on  $C_{dis}$ , and thus on  $TC$ , can still be significant.

Figure 9a shows the indication of  $C_{dis}$  in *SE1* (halved atmospheric heat diffusivity), given by the runs with fast gas exchange 20 for  $CO_2$ . We see a signal of positive  $C_{dis}$  originating in the Southern Ocean that is much more pronounced in *SE1* compared to the control *PIES278* (Fig 9c). *SE1* is by far the coldest state and the global percentage of sea ice cover is doubled compared to *PIES278* (for reference, in the second coldest state the sea ice cover has increased by less than 40 % compared to *PIES278*, see Table 2). It is likely that the extensive sea ice in *SE1*, to a larger extent than in the control, prevents the oversaturated deepwater from equilibrating with the atmosphere before sinking again. For *SE1*, the analysis of the run with artificially fast 25 gas exchange reveals that the contribution of  $C_{dis}$  to  $C_{res}$  is large enough in this case to be critical for the sign of  $\Delta TC$  (see *SE1* in Figure 2); it shifts from being  $+0.64 \cdot 10^{16}$  mol with normal gas exchange to being  $-0.43 \cdot 10^{16}$  mol when the gas exchange is artificially fast.

Comparing panels b and c in Figure 9, we see that the differences are more difficult to attribute to one single process. The overturning circulation in *SE4* is stronger than in *PIES278*. This makes the global ocean warmer, reduces sea ice, but 30 also shortens the time for equilibration with the atmosphere in the North Atlantic branch. In this particular case of stronger circulation, the shorter time for equilibration dominates over the reduced temperature gradient and causes more negative disequilibrium in the North Atlantic deepwater formation area compared to the control in panel c. In the Southern Ocean, there is less sea ice, which allows more direct contact between the ocean and the atmosphere. However, due to the faster overturning, the deep waters that upwell here will quickly sink again. This is particularly seen in the Pacific sector, as a band of positive



$C_{dis}$  extending from the surface and down, whereas in the control, the positive  $C_{dis}$  is more confined to just below the sea ice area.

#### 4.2 Step 2 - Drawdown potential

In this step, we use the set of equilibrium states ( $SE$ :s and the control  $PIES278$ ) from step 1 as initial states for determining the drawdown potential,  $DP$  (Fig. 1). This reveals the dependence of the resulting equilibrium state  $DE1 - DE12$  on differences in the initial states  $SE1 - SE12$ . The control drawdown equilibrium is denoted  $CDE$ .  $DP$  is computed as the difference in  $pCO_2^{atm}$  between 278 ppm and the drawdown equilibrium states.

The  $DP$  varies strongly between the ensemble members. We see that  $DP$  is close to linearly related to the biological efficiency, in terms of  $\overline{P}^*$ , of the initial equilibrium state (Fig. 6 c). The near linear relationship between  $DP$  and  $\overline{P}^*$  of the initial  $SE$  is expected (see e.g. Marinov et al. (2008a)). If the biological efficiency in the  $SE$  is small, there is a larger pool of unused nutrients that can be used to capture carbon when biological efficiency is increased to 100 %. In this ensemble, an increase in biological efficiency manifested by an increase in  $\overline{P}^*$  of 0.1, corresponds to a drawdown of  $CO_2$  from the atmosphere of about 20-30 ppm. This is similar to the theoretical prediction by Ito and Follows (2005) of  $\sim 30$  ppm.

However, the drawdown of atmospheric  $CO_2$  achieved during the drawdown experiments is not purely due to biology. There are also indirect effects on  $pCO_2^{atm}$  due to changes in ocean temperature caused by changes in radiative balance, circulation and disequilibrium. Hence, we can not expect the model results to correspond exactly to the theoretical prediction in this case. The most prominent example is  $SE1$ , which has a low initial  $\overline{P}^*$ , but still has a low  $DP$ . This is the coldest of all initial states, with very high ocean sea ice cover (Table 2) compared to the other  $SE$ :a, and the cold conditions are likely to be affecting the conditions for biological production. Another example is that the near-linear relationship between  $\overline{P}^*$  and  $DP$  does not predict  $DP$  to be exactly zero for  $\overline{P}^* = 1$ , as would have to be the case.

There is a tendency that those experiments that have a lower  $T_{avg}$  (thus a larger inventory of  $C_{sat}$ ) compared to  $PIES278$  have a smaller  $DP$  than those with higher temperatures (Fig. 10). This has to do with circulation changes acting in a predictable way. The circulation change that is causing a colder temperature is also causing the OVT to be weaker, and at the same time causing a more efficient biological pump (more  $C_{soft}$  and higher  $\overline{P}^*$ ) and hence a smaller  $DP$  (Fig. 10). When OVT is weaker, there is more time for biology to take up nutrients and there is hence less preformed nutrients left at the surface, which means the  $DP$  will be smaller.

When compared to the  $CDE$ , there are two exceptions to the rule of colder temperatures in the initial state being associated with a smaller  $DP$  and warmer temperatures being associated with a larger  $DP$ ; 1)  $DE3$  (cyan star in Fig. 10), where the circulation in the initial state  $SE3$  is slightly weaker than the control  $PIES278$  (see Table S1 and Fig. 4). In this experiment, the Southern Ocean cell retreats while the NADW-cell expands. Since temperatures in the North Atlantic are higher,  $T_{avg}$  increases. In this case,  $DP$  is smaller, as expected for a case with weaker circulation. 2)  $DE10$  (yellow square in Fig. 10), where the circulation in the initial state  $SE10$  is stronger, but the global ocean temperature is in fact lower, than in the control  $PIES278$ , due to the expansion of the Southern Ocean cell. However,  $DP$  is still larger, as expected in a case with stronger circulation.



## 5 Discussion

### 5.1 Solubility pump and disequilibrium

The effect on  $pCO_2^{atm}$  of a change in the solubility pump is approximately quantifiable from the change in global ocean average temperature,  $\Delta T_{avg}$ , between two simulations, as described by Eq. (A9) suggested by Goodwin et al. (2011). According to 5 this equation, the span of  $\Delta T_{avg}$  in our ensemble would correspond to 9.1–11.1 ppm  $^{\circ}\text{C}^{-1}$  (linear fit: 9.8 ppm  $^{\circ}\text{C}^{-1}$  ). Solving the carbon system for the same span of  $\Delta T_{avg}$  yields 12.5–13.1 ppm  $^{\circ}\text{C}$  (linear fit: 12.9 ppm  $^{\circ}\text{C}^{-1}$  ). The error in using the simplified equation seems to be on the order of 20 %. Depending on which process is causing the change in ocean circulation, the impact of changes in the solubility pump on  $pCO_2^{atm}$  can be almost as important as the impact of changes in the biological 10  $\text{CO}_2$  efficiency of carbon uptake. For changes in ocean horizontal diffusivity, the solubility pump effect is even the dominant response. In previous studies, this has to some extent been disregarded, when the response of the biological pump has been assumed to be the dominant response to the applied changes in circulation (e.g., Archer et al., 2000a; Kwon et al., 2011).

It has been more difficult to quantify the effects of  $\text{CO}_2$  disequilibrium, but in this model it appears to be particularly important in simulations with a lot of sea ice (e.g. *SE1*). This leads us to the conclusion that it may also be of importance in glacial simulations. A caveat to this finding is cGENIE's coarse resolution at high latitudes, and its simplified representation 15 of sea ice as a complete barrier to gas exchange. If we assume that calculation errors are small, and thus that  $\Delta C_{res}$  is mainly due to  $\Delta C_{dis}$ , the circulation changes we impose would contribute  $\sim 10$ –30 ppm of atmospheric  $\text{CO}_2$ , which is comparable to the results of Marinov et al. (2008a).

### 5.2 Implications for model validation

When comparing model studies, it is important to recognize differences in biological efficiency in their control states. The 20 pre-industrial  $\overline{P}^*$  of a model will determine its pre-industrial inventory of  $C_{soft}$  but also its drawdown potential. If the pre-industrial  $\overline{P}^*$  is incorrect, the total carbon inventory in the model will adjust to compensate this error, in order to achieve equilibrium with pre-industrial  $pCO_2^{atm}$ . Hence, failing to tune the models for pre-industrial  $\overline{P}^*$  will mean that they start from a non-representative state of the carbon system. Thus, models with different initial  $\overline{P}^*$  will have different  $\Delta pCO_2$  in response to similar circulation changes. This point was mentioned in Marinov et al. (2008a), but does not seem to have been picked 25 up in the model intercomparison community and, still, models are not tuned for  $\overline{P}^*$ . The range of  $\overline{P}^*$  in our pre-industrial ensemble (*SE1*–*SE12*) is 0.34–0.62. This range includes the current estimate for the global ocean, which according to Ito and Follows (2005) is 0.36. Our range in initial state  $\overline{P}^*$  corresponds to a range in drawdown potential of 94–139 ppm. While using a different model, but a similar approach, we confirm the conclusion of Marinov et al. (2008a) and want to stress the importance of a similar initial efficiency of the biological pump in model intercomparison studies where  $\text{CO}_2$  drawdown is 30 diagnosed.

Few studies have simultaneously diagnosed the individual contributions by the solubility and biological pumps and the effect of surface  $\text{CO}_2$  disequilibrium. Studies by Lauderdale et al. (2013) and Bernardello et al. (2014) use a similar separation of the carbon storage processes as we do. For increases in wind stress, the sign of  $\Delta TC$  (and thus of  $\Delta pCO_2^{atm}$ ) and the



individual contributions by the carbon pumps and  $C_{dis}$  agree with those found by Lauderdale et al. (2013). Compared to the scenario-specific results of Bernardello et al. (2014), our results could be used more generally as a way of anticipating the model behaviour, based on in which way the ocean circulation changes in a model study. Depending on in which way we have changed the ocean forcing, and what the resulting effect on ocean circulation is, the origin of the change in ocean carbon storage is different. When wind stress or ocean vertical diffusivity is changed, the response of the biological pump gives the most important effect on ocean carbon storage, whereas when atmospheric heat diffusivity or ocean horizontal diffusivity is changed, the solubility pump and the disequilibrium component are also important and sometimes dominant. Our results give a first approximation of the effect of these ocean circulation changes on the ocean carbon storage, but it is important to keep in mind that the results of changes in individual parameters do not always combine linearly. For example, in the case of halved winds combined with low ocean vertical diffusivity (SE12), we see that the response of the biological pump in the combined case is more or less a linear combination of the cases where these changes were made individually (SE:s 3 and 5 respectively). However, the solubility pump behaves in the same way as in the case with low ocean vertical diffusivity and control state winds (SE5). This is because the low ocean vertical diffusivity is more important for the global ocean mean temperature, and thus for the solubility pump, than the surface wind stress.

### 15 5.3 Implications for glacial studies

We have shown that, when comparing model simulations with the same  $pCO_2^{atm}$ , but with differences in ocean circulation and AMOC strength, the compared simulations will have different carbon inventories, and different strengths of the ocean carbon pumps. In the PMIP3 intercomparison project, where glacial simulations with different models are compared, the models are forced with glacial  $pCO_2^{atm}$  to achieve the LGM state (<https://pmip3.lsce.ipsl.fr/>). The ocean circulation state is however not specified. Otto-Bliesner et al. (2007) showed that model simulations in the PMIP2 project developed very different LGM ocean circulation patterns and specifically large differences in AMOC strength, despite displaying similar ocean circulation patterns in pre-industrial simulations. Most models in the studied ensemble had been initiated with pre-industrial circulation and LGM boundary conditions according to the PMIP2 protocol. When run to quasi-equilibrium, some models would develop an LGM-like circulation (when compared to proxy data) and some would keep a more pre-industrial like simulation. Since the ocean circulation patterns differ, the ocean carbon storage and thus the model carbon inventories of the compared PMIP-simulations also differ. This will be important when comparing e.g. deglacial scenarios run with these different models (e.g., Zhang et al., 2013).

When attempting to simulate the glacial CO<sub>2</sub> drawdown, it is crucial to critically evaluate the changes in forcing that need to be applied to achieve a glacial state in the model. We should ask ourselves whether these changes agree with what we believe 30 actually happened in the climate system during a glacial.

When applying PMIP3 boundary conditions for the LGM, the height of the ice sheet in the northern hemisphere will tend to intensify both the wind stress over the North Atlantic basin and as a result the AMOC-circulation (Muglia and Schmittner, 2015). Similar effects on the wind fields due to the Laurentide ice sheet are seen in e.g. Löfverström et al. (2014). Sime et al. (2013) suggest that Southern Hemisphere winds will also be stronger when applying LGM boundary conditions, though they



emphasise that results from different palaeoproxies and models disagree on this. In our simulation, we intensify the wind stress in both hemispheres and this leads to decreased capacity of both the biological and the solubility pump, and effectively an increase in  $pCO_2^{atm}$ . Lauderdale et al. (2013) showed similar results, but for increased Southern Ocean winds. Hence, the changes in wind fields achieved by the applied LGM boundary conditions in models may be contributing to the difficulties in 5 simulating the glacial decrease in  $pCO_2^{atm}$ .

In those of our ensemble members where ocean vertical diffusivity is halved, we achieve some glacial-like ocean characteristics; the circulation is weaker, the global ocean temperature is colder and the biological pump is stronger. However, it has been shown by Schmittner et al. (2015) that open ocean mixing is likely to have been intensified during glacials, when lower sea level made shelf areas decrease and tidal mixing was shifted to the deep ocean. In their model, global ocean mean 10 vertical diffusivity increased by more than a factor of 3, leading to an intensification of ocean overturning. In our experiments, a doubling of vertical diffusivity leads to a decrease in ocean carbon storage corresponding to an increase of  $pCO_2^{atm}$  of more than 20 ppm (see *SE6* in Figure 2). Hence, in a full glacial scenario, processes causing increased ocean carbon storage would have to offset this effect before causing any net decrease in  $pCO_2^{atm}$ . Other effects on glacial  $pCO_2^{atm}$  linked to lower sea level 15 (reduced ocean volume) during glacials, caused by higher salinity, and higher concentration of DIC, alkalinity and nutrients, have been constrained to +12–16 ppm (Köhler and Fischer, 2006; Brovkin et al., 2007; Kohfeld and Ridgwell, 2009). In this process study we are not aiming to reproduce LGM conditions in the model and such effects of changes in ocean volume are beyond the scope of our investigations. Ocean volume, and global averages of salinity, alkalinity and phosphate have thus been 20 kept constant in our simulations.

Since numerous studies of proxy data indicate that the global ocean was in fact less ventilated during glacials (e.g., Broecker et al., 1990; Sikes et al., 2000; Keigwin and Schlegel, 2002; Skinner et al., 2010, 2015), it seems possible that the effect of increased mixing was indeed offset by some other process. One such factor could be that the global ocean was saltier and more stratified (Ballarotta et al., 2014). In our simulations, weaker overturning circulation is also connected to colder temperatures. These cold simulations show a tendency towards lower drawdown potentials. It is likely that the more sluggish circulation is 25 already allowing a more efficient biological pump, leading to a higher  $\overline{P}^*$  and thus a smaller drawdown potential.

## 25 6 Conclusions

In this paper, we have studied three mechanisms for ocean carbon storage — the biological pump, the solubility pump and the contribution from air-sea  $CO_2$  disequilibrium — and quantified the response of these mechanisms to differences in the equilibrium ocean circulation state. For a given set of equilibrium states in the model cGENIE, we have constrained the response of the carbon storage associated with the first two mechanisms reasonably well and diagnosed their influence on 30  $pCO_2^{atm}$ . We have also seen some response related to ocean  $CO_2$  disequilibrium.

We have obtained different states of equilibrium ocean circulation by varying forcings and model parameters (listed in Table 1) in a model ensemble. This was not done with the aim to achieve a glacial-like circulation, but to study how the ocean carbon storage responds to changes in a wide range of circulation processes. We change forcing parameters such as wind stress, ocean



diffusivity and atmospheric heat diffusivity and run the model to equilibrium while keeping atmospheric CO<sub>2</sub> constant. We study the response of the three mechanisms for ocean carbon storage and relate it to differences in ocean circulation strength. In cases with weaker circulation, we see that the ocean's capacity for carbon storage is larger. The contributions to the change in carbon storage by the solubility pump, the biological pump or CO<sub>2</sub> disequilibrium are different depending on the origin of  
5 the ocean circulation change. When wind stress or ocean vertical diffusivity is changed, the response of the biological pump has the strongest impact on ocean carbon storage. In contrast, when atmospheric heat diffusivity or ocean horizontal diffusivity is changed, the solubility pump and the disequilibrium component also give important, and sometimes dominant, contributions to the change in ocean carbon storage.

Finally, to constrain the biological pump, we used the *SE* ensemble members (Fig. 1) as initial states to see how their  
10  $pCO_2^{atm}$  responded when the model was forced into a state with 100 % efficient biology. We applied similar adjustments to circulation parameters as those tested in Marinov et al. (2008b), in order to allow some direct comparison of our results with their study. In agreement with Marinov et al. (2008b), we find that the drawdown potential of an ensemble member is a direct result of its biological efficiency, as measured by the ratio between global average regenerated ( $\overline{P}_{reg}$ ) and total ( $\overline{P}$ ) phosphorus, denoted  $\overline{P}^*$ , in its initial equilibrium state.

15 This study shows that, a model's control pre-industrial state will determine the sensitivity of the mechanisms for ocean carbon storage to changes in biological efficiency. Often, a model with stronger circulation will have a higher global ocean mean temperature, thus a weaker solubility pump, and lower biological efficiency, thus also a weaker biological pump. This leads to that model having a smaller ocean carbon inventory in the control state, but a larger drawdown potential for CO<sub>2</sub>, compared to a model with weaker circulation. Hence, when different models are used to simulate a glacial scenario, it is likely  
20 that a significant part of the difference in their CO<sub>2</sub> drawdown potentials results from differences that are already present, but not directly visible, in their control states. This has potentially important implications for model intercomparison studies.

In our entire ensemble of simulations, 100 % nutrient utilisation efficiency causes more drawdown than necessary to reach glacial values. Future efforts need to deduce how big an increase in nutrient utilisation we could expect for a glacial, when using proxy data of e.g. iron fertilisation (e.g., Petit et al., 1999) and water mass properties (e.g. Elderfield and Rickaby, 2000)  
25 as a constraint. By understanding how ocean circulation changes during the glacials may have contributed to altering the ocean nutrient utilisation efficiency, it will be easier to quantify how much it may have increased due to e.g. fertilisation by deposition of iron from dust. However, recent studies have shown that there may have been more, not less, preformed nutrients in the deep ocean during the last glacial, which implies less efficient nutrient utilisation by biology Homola et al. (2015). One aspect that could explain how more carbon could still be trapped by biology in such a case is if the stoichiometric ratios in a glacial  
30 scenario no longer follow the averages described by Redfield (1963). In most climate models, this is currently not taken into account. Implementation of variable stoichiometry in models could however bring interesting insights in the future.



*Code and data availability.* The source code for cGENIE is publically available at <http://www.seao2.info/mycgenie.html>. For this work, modifications have been made to the gas exchange code in the file biogem\_box.f90 and the modified version is provided for download with this manuscript. Data is available upon request (e-mail to the corresponding author).

## Appendix A: Corresponding changes in $pCO_2^{atm}$

5 To achieve the equilibrium states of our ensemble ( $SE1 - SE12$ ), we have been restoring  $pCO_2^{atm}$  to 278  $\mu\text{atm}$  ( $\mu\text{atm} \approx \text{ppm}$ ). This means that the changes in carbon cycling caused by the imposed circulation changes are only seen as changes in ocean carbon storage. In the real world, we would also get an effect on the air-sea equilibrium and on  $pCO_2^{atm}$ .

In this section, we translate the observed changes in the ocean  $TC$ ,  $C_{sat}$ ,  $C_{soft}$ ,  $C_{carb}$ , and  $C_{res}$  to the effect on  $pCO_2^{atm}$  that would have been seen if it had not been restored. The fact that we are indeed changing the total carbon inventory of the 10 system means that these translations are approximate, since they assume the inventory to be constant. However, the changes in inventory are small compared to the size of the total inventory and therefore these calculations are still reasonably correct.

First, we need to know the Revelle buffer factor,  $R_C$ , for the control equilibrium, where  $R_C$  is

$$R_C = \frac{\Delta[CO_2]}{[CO_2]} / \frac{\Delta[DIC]}{[DIC]} \approx \frac{\Delta[CO_2]}{[CO_2]} / \frac{\Delta[TC]}{[TC]} \quad (\text{A1})$$

where  $[CO_2]$  and  $[DIC]$  are the concentrations of dissolved  $CO_2$  and DIC in the surface ocean. The difference between  $[TC]$  15 and  $[DIC]$  is very small and is due to the carbon trapped in organic molecules. This difference is small enough to be negligible in these calculations, and henceforth we consider  $DIC$  and  $TC$  to be directly interchangeable in all equations.

$R_C$  is calculated by using the carbon system equation solver CO2SYS (Lewis et al., 1998). As input we use the control equilibrium global averages of temperature, salinity and concentrations of  $A_{pre}$  and  $PO_4$ , which are 3.58  $^{\circ}\text{C}$ , 34.90, 2296  $\mu\text{mol kg}^{-1}$ , 2.15  $\mu\text{mol kg}^{-1}$  respectively.  $R_C$  is given as output from CO2SYS. Given the control  $pCO_2^{atm}$  of 278 ppm,  $R_C$  is 20 12.4, which we then use as  $R_C$  in the rest of our calculations. From the equation solver, we also get the global average ocean concentration of  $DIC$  that corresponds to the given conditions. We call this concentration  $DIC_{ref}$  and it is 2100  $\mu\text{mol kg}^{-1}$ .

$DIC_{ref}$  is used as input when we next prepare to calculate the alkalinity factor,  $R_A$ , of the system. This factor is used to calculate the effect of a change in alkalinity on  $pCO_2^{atm}$ .  $R_A$  is given by

$$R_A = \frac{\Delta[CO_2]}{[CO_2]} / \frac{\Delta[A_{pre}]}{[A_{pre}]} \quad (\text{A2})$$

25 Again, we use CO2SYS, with the same control state equilibrium parameters as before, but now giving  $DIC_{ref}$  instead of  $pCO_2^{atm}$ . This time we get a value for  $pCO_2^{atm}$  as output. We will denote this output  $pCO_{2_{alk}}$ . We also let CO2SYS calculate  $pCO_2^{atm}$  for a 1 % increase in  $\overline{A_{pre}}$ .  $pCO_{2_{alk}}$  is 278 ppm in the case with all control values and 248 ppm in the case with increased  $A_{pre}$ . We take the average of these two calculations, 263 ppm, as  $\overline{pCO_{2_{alk}}}$  and  $\Delta pCO_{2_{alk}} = 278 - 248 = 30 \text{ ppm}$ . With these values, Eq. (A2) gives  $R_A = -11.4$ .



We can now calculate how a change in  $TC$ , in our  $SE$  ensemble would affect  $pCO_2^{atm}$ , if we were not restoring it:

$$\Delta pCO_2^{atm} \Big|_{TC} = pCO_2^{atm} \cdot -\left(R_C \frac{\Delta TC}{TC} + R_A \frac{\Delta Alk}{Alk}\right) \quad (A3)$$

Here,  $\Delta TC$  is the change in  $TC$  of an ensemble member ( $SE1 - SE12$ ) c.f. the control, as seen in panel a of Figure 2.  $TC$  and  $Alk$  are total inventories of carbon and alkalinity respectively in the control equilibrium and  $\Delta Alk$  is the difference in 5 alkalinity inventory between the ensemble member and the control. In this ensemble,  $\Delta Alk$  is solely due to changes in the biological pump.

The effect a change in the inventory of residual carbon,  $M_o \cdot \Delta C_{res}$ , would have on  $pCO_2^{atm}$ , is calculated in a similar manner as for  $\Delta TC$ :

$$\Delta pCO_2^{atm} \Big|_{C_{res}} = pCO_2^{atm} \cdot -R_C \frac{M_o \Delta C_{res}}{TC} \quad (A4)$$

10 Since the biological pump is not involved in this change, we need not take into account changes related to alkalinity, and therefore that term is removed.

We estimate the effects of changes in the biological pump using equations from Kwon et al. (2011), which they base on the framework described in Ito and Follows (2005). They make simplifications assuming that  $[C_{sat}]$  can replace  $[DIC]$  in Eq. (A1), and that, to leading order approximation, the sensitivity of  $pCO_2^{atm}$  to changes in  $C_{soft}$  is independent of the size of the 15 carbon reservoirs in the atmosphere and ocean respectively. These simplifications yield Eqs. (A5) and (A7).

$$\Delta pCO_2^{atm} \Big|_{C_{soft}} = pCO_2^{atm} \cdot \Delta \overline{C_{soft}} \cdot C_{soft_F} \quad (A5)$$

$$C_{soft_F} = \frac{-R_C}{\overline{C_{sat}}} + R_{N:C} \frac{R_A}{\overline{A_{pre}}} \quad (A6)$$

Equation (A5) gives the change in  $pCO_2^{atm}$  that would correspond to an observed  $\Delta C_{soft}$ .  $\Delta \overline{C_{soft}}$  is the change in global 20 average concentration of  $C_{soft}$  in the control equilibrium and  $C_{soft_F}$  is the scaled buffer factor for  $C_{soft}$ , which is based on global average concentrations of  $C_{sat}$  and  $A_{pre}$  (see Kwon et al. (2011)). The approximation in this case that  $pCO_2^{atm}$  is insensitive to the size of the carbon reservoirs in the atmosphere and ocean overestimates the excursion in  $pCO_2^{atm}$  due to changes in  $C_{soft}$  by about 10–15 %.

For  $C_{carb}$ , the corresponding equations are

$$\Delta pCO_2^{atm} \Big|_{C_{carb}} = pCO_2^{atm} \cdot \Delta \overline{C_{carb}} \cdot C_{carb_F} \quad (A7)$$

$$25 \quad C_{carb_F} = \frac{-R_C}{\overline{C_{sat}}} - 2 \frac{R_A}{\overline{A_{pre}}} \quad (A8)$$



The only remaining carbon species is  $C_{sat}$ . We calculate the effects on  $pCO_2^{atm}$  corresponding to our observed  $\Delta C_{sat}$  directly by solving the carbon system equations using CO2SYS. As input data we use the observed salinity, global average concentration of  $DIC$  and surface  $PO_4$  of the control equilibrium, as well as the restored value of  $pCO_2^{atm} = 278$  ppm. We run CO2SYS with the control global average temperature and the  $SE$  ensemble member global average temperature. As output, 5 we then get the  $pCO_2^{atm}$  at these two temperatures. Thus, we can compute the  $\Delta pCO_2^{atm}$  we would get as a result of solely changing the temperature and keeping everything else but  $pCO_2^{atm}$  constant.

Instead of solving the carbon system equations to get the change in  $pCO_2^{atm}$ , Goodwin et al. (2011) suggest using a simplified equation, where the fractional change  $\Delta pCO_2^{atm}/pCO_2^{atm}$ , is described as proportional to a function of global average ocean temperature;

$$10 \quad \frac{\Delta pCO_2^{atm}}{pCO_2^{atm}} \sim -\frac{V}{I_B} \frac{\partial C_{sat}}{\partial T} \Delta T_{avg} \quad (A9)$$

$$I_B = I_A + I_O / R_{global} \quad (A10)$$

Here,  $V$  is the ocean volume ( $m^3$ ) and  $\frac{\partial C_{sat}}{\partial T}$  ( $\text{mol m}^{-3} \text{ }^{\circ}\text{C}^{-1}$ ) is the change in saturation concentration of DIC per unit change of seawater temperature, in this case global ocean average temperature.  $I_B$  is the buffered amount of carbon in the system, or in other words the  $\text{CO}_2$  that is “available for redistribution between the atmosphere and ocean” (Goodwin et al., 2007). As 15 described by Eq. (A10),  $I_B$  is based on the atmospheric carbon inventory,  $I_A$ , and the ocean inventory of DIC,  $I_O$ , scaled by the global value for the Revelle buffer factor, which in this case is the same as  $R_C$  above.

*Author contributions.* M. Ödalen, J. Nycander and K. I. C. Oliver designed the model experiments. A. Ridgwell developed the cGENIE model code, and M. Ödalen adapted it for the experimental design. M. Ödalen performed the model simulations and produced the figures. L. Brodeau provided technical expertise for the model setup. M. Ödalen prepared the manuscript with contributions from all co-authors.

20 *Competing interests.* No competing interests are present.

*Acknowledgements.* The simulations were performed on resources provided by the Swedish National Infrastructure for Computing (SNIC) at the National Supercomputer Centre, Linköping University. Kevin Oliver would like to acknowledge the support by UK NERC grant NE/K002546/1 and he is grateful to the International Mereorological Institute for generous support during several visists to Stockholm. This work benefited from helpful discussions with Johan Nilsson.



## References

Anderson, L. A. and Sarmiento, J. L.: Redfield ratios of remineralization determined by nutrient data analysis, *Global biogeochemical cycles*, 8, 65–80, 1994.

Archer, D., Winguth, A., Lea, D., and Mahowald, N.: What caused the glacial/interglacial atmospheric pCO<sub>2</sub> cycles?, *Reviews of Geophysics*, 38, 159–189, 2000a.

Archer, D. E., Eshel, G., Winguth, A., Broecker, W., Pierrehumbert, R., Tobis, M., and Jacob, R.: Atmospheric pCO<sub>2</sub> sensitivity to the biological pump in the ocean, *Global Biogeochemical Cycles*, 14, 1219–1230, 2000b.

Aumont, O., van Hulten, M., Roy-Barman, M., Dutay, J.-C., Ethé, C., and Gehlen, M.: A reactivity continuum of particulate organic matter in a global ocean biogeochemical model, *Biogeosciences Discussions*, 2016, 1–37, doi:10.5194/bg-2016-374, <http://www.biogeosciences-discuss.net/bg-2016-374/>, 2016.

Ballarotta, M., Falahat, S., Brodeau, L., and Döös, K.: On the glacial and interglacial thermohaline circulation and the associated transports of heat and freshwater, *Ocean Science*, 10, 907, 2014.

Bernardello, R., Marinov, I., Palter, J. B., Sarmiento, J. L., Galbraith, E. D., and Slater, R. D.: Response of the ocean natural carbon storage to projected twenty-first-century climate change, *Journal of Climate*, 27, 2033–2053, 2014.

Broecker, W. S.: "NO", A conservative water-mass tracer, *Earth and Planetary Science Letters*, 23, 100–107, 1974.

Broecker, W. S.: Glacial to interglacial changes in ocean chemistry, *Progress in Oceanography*, 11, 151 – 197, doi:[http://dx.doi.org/10.1016/0079-6611\(82\)90007-6](http://dx.doi.org/10.1016/0079-6611(82)90007-6), <http://www.sciencedirect.com/science/article/pii/0079661182900076>, 1982.

Broecker, W. S., Peng, T.-H., Trumbore, S., Bonani, G., and Wolfli, W.: The distribution of radiocarbon in the glacial ocean, *Global Biogeochemical Cycles*, 4, 103–117, 1990.

Brovkin, V., Ganopolski, A., Archer, D., and Rahmstorf, S.: Lowering of glacial atmospheric CO<sub>2</sub> in response to changes in oceanic circulation and marine biogeochemistry, *Paleoceanography*, 22, 2007.

Cao, L., Eby, M., Ridgwell, A., Caldeira, K., Archer, D., Ishida, A., Joos, F., Matsumoto, K., Mikolajewicz, U., Mouchet, A., et al.: The role of ocean transport in the uptake of anthropogenic CO<sub>2</sub>, *Biogeosciences*, 6, 375–390, 2009.

Comiso, J. C.: Variability and trends of the global sea ice cover, in: *Sea ice: an introduction to its physics, chemistry, biology and geology*, edited by Thomas, D. N. and Dieckmann, G. S., John Wiley & Sons, 2008.

Edwards, N. R. and Marsh, R.: Uncertainties due to transport-parameter sensitivity in an efficient 3-D ocean-climate model, *Climate Dynamics*, 24, 415–433, 2005.

Elderfield, H. and Rickaby, R.: Oceanic Cd/P ratio and nutrient utilization in the glacial Southern Ocean, *Nature*, 405, 305–310, 2000.

Eriksson, E. and Welander, P.: On a Mathematical Model of the Carbon Cycle in Nature, *Tellus*, 8, 155–175, doi:10.1111/j.2153-3490.1956.tb01207.x, <http://dx.doi.org/10.1111/j.2153-3490.1956.tb01207.x>, 1956.

Falkowski, P., Scholes, R. J., Boyle, E., Canadell, J., Canfield, D., Elser, J., Gruber, N., Hibbard, K., Högberg, P., Linder, S., Mackenzie, F. T., Moore III, B., Pedersen, T., Rosenthal, Y., Seitzinger, S., Smetacek, V., and Steffan, W.: The Global Carbon Cycle: A Test of Our Knowledge of Earth as a System, *Science*, 290, 291–296, doi:10.1126/science.290.5490.291, <http://science.sciencemag.org/content/290/5490/291>, 2000.

Galbraith, E. D. and Martiny, A. C.: A simple nutrient-dependence mechanism for predicting the stoichiometry of marine ecosystems, *Proceedings of the National Academy of Sciences*, 112, 8199–8204, 2015.



Ganopolski, A., Calov, R., and Claussen, M.: Simulation of the last glacial cycle with a coupled climate ice-sheet model of intermediate complexity, *Climate of the Past*, 6, 229–244, 2010.

Goodwin, P., Williams, R. G., Follows, M. J., and Dutkiewicz, S.: Ocean-atmosphere partitioning of anthropogenic carbon dioxide on centennial timescales, *Global Biogeochemical Cycles*, 21, 2007.

5 Goodwin, P., Follows, M. J., and Williams, R. G.: Analytical relationships between atmospheric carbon dioxide, carbon emissions, and ocean processes, *Global Biogeochemical Cycles*, 22, 2008.

Goodwin, P., Oliver, K. I. C., and Lenton, T. M.: Observational constraints on the causes of Holocene CO<sub>2</sub> change, *Global Biogeochemical Cycles*, 25, n/a–n/a, doi:10.1029/2010GB003888, <http://dx.doi.org/10.1029/2010GB003888>, gB3011, 2011.

Hain, M. P., Sigman, D. M., and Haug, G. H.: Carbon dioxide effects of Antarctic stratification, North Atlantic Intermediate Water formation, 10 and subantarctic nutrient drawdown during the last ice age: Diagnosis and synthesis in a geochemical box model, *Global Biogeochemical Cycles*, 24, 2010.

Headly, M. A. and Severinghaus, J. P.: A method to measure Kr/N<sub>2</sub> ratios in air bubbles trapped in ice cores and its application in reconstructing past mean ocean temperature, *Journal of Geophysical Research: Atmospheres*, 112, n/a–n/a, doi:10.1029/2006JD008317, <http://dx.doi.org/10.1029/2006JD008317>, d19105, 2007.

15 Homola, K., Spivack, A. J., D'Hondt, S., Estes, E. R., Insua, T. L., McKinley, C. C., Murray, R. W., Pockalny, R. A., Robinson, R. S., and Sauvage, J.: Preformed Nitrate in the Glacial North Atlantic, *AGU Fall Meeting Abstracts*, 2015.

IPCC: Contribution of Working Group I to the Fourth Assessment Report of the Intergovernmental Panel on Climate Change, 2007.

Ito, T. and Follows, M. J.: Preformed phosphate, soft tissue pump and atmospheric CO<sub>2</sub>, *Journal of Marine Research*, 63, 813–839, 2005.

Keigwin, L. and Schlegel, M.: Ocean ventilation and sedimentation since the glacial maximum at 3 km in the western North Atlantic, 20 Geochemistry, *Geophysics, Geosystems*, 3, 1–14, 2002.

Kohfeld, K. E. and Ridgwell, A.: Glacial-Interglacial Variability in Atmospheric CO<sub>2</sub>, in: *Surface Ocean-Lower Atmosphere Processes*, edited by Le Quéré, C. and S., S. E., pp. 251–286, American Geophysical Union, Washington D.C., 2009.

Köhler, P. and Fischer, H.: Proposing a mechanistic understanding of changes in atmospheric CO<sub>2</sub> during the last 740 000 years, *Climate of the Past Discussions*, 2, 1–42, 2006.

25 Kwon, E. Y., Sarmiento, J. L., Toggweiler, J., and DeVries, T.: The control of atmospheric pCO<sub>2</sub> by ocean ventilation change: The effect of the oceanic storage of biogenic carbon, *Global Biogeochemical Cycles*, 25, 2011.

Lauderdale, J. M., Garabato, A. C. N., Oliver, K. I. C., Follows, M. J., and Williams, R. G.: Wind-driven changes in Southern Ocean residual circulation, ocean carbon reservoirs and atmospheric CO<sub>2</sub>, *Climate dynamics*, 41, 2145–2164, 2013.

Lewis, E., Wallace, D., and Allison, L. J.: Program developed for CO<sub>2</sub> system calculations, ORNL/CDIAC-105, Carbon Dioxide Information 30 Analysis Center, managed by Lockheed Martin Energy Research Corporation for the US Department of Energy Tennessee, 1998.

Locarnini, R. A., Mishonov, A. V., Antonov, J. I., Boyer, T. P., Garcia, H. E., Baranova, O. K., Zweng, M. M., Paver, C. R., Reagan, J. R., Johnson, D. R., Hamilton, M., and Seidov, D.: World Ocean Atlas 2013, Volume 1: Temperature, Tech. Rep. 73, NOAA Atlas NESDIS, 40 pp., 2013.

Löfverström, M., Caballero, R., Nilsson, J., and Kleman, J.: Evolution of the large-scale atmospheric circulation in response to changing ice 35 sheets over the last glacial cycle, *Climate of the Past*, 10, 1453–1471, 2014.

Lüthi, D. et al.: EPICA Dome C Ice Core 800KYr Carbon Dioxide Data, IGBP PAGES/World Data Center for Paleoclimatology Data Contribution Series, 55, 2008.



Marinov, I., Follows, M., Gnanadesikan, A., Sarmiento, J. L., and Slater, R. D.: How does ocean biology affect atmospheric pCO<sub>2</sub>? Theory and models, *Journal of Geophysical Research*, 113, 2008a.

Marinov, I., Gnanadesikan, A., Sarmiento, J. L., Toggweiler, J. R., Follows, M., and Mignone, B. K.: Impact of oceanic circulation on biological carbon storage in the ocean and atmospheric pCO<sub>2</sub>, *Global Biogeochemical Cycles*, 22, 2008b.

5 Marsh, R., Sobester, A., Hart, E. E., Oliver, K., Edwards, N., and Cox, S.: An optimally tuned ensemble of the "eb\_go\_gs" configuration of GENIE: parameter sensitivity and bifurcations in the Atlantic overturning circulation, *Geoscientific Model Development*, 6, 1729–1744, 2013.

Muglia, J. and Schmittner, A.: Glacial Atlantic overturning increased by wind stress in climate models, *Geophysical Research Letters*, 42, 9862–9868, 2015.

10 Müller, S. A., Joos, F., Edwards, N. R., and Stocker, T. F.: Water Mass Distribution and Ventilation Time Scales in a Cost-Efficient, Three-Dimensional Ocean Model, *Journal of Climate*, 19, 5479–5499, doi:10.1175/JCLI3911.1, <http://dx.doi.org/10.1175/JCLI3911.1>, 2006.

Otto-Blienes, B. L., Hewitt, C. D., Marchitto, T. M., Brady, E., Abe-Ouchi, A., Crucifix, M., Murakami, S., and Weber, S. L.: Last Glacial Maximum ocean thermohaline circulation: PMIP2 model intercomparisons and data constraints, *Geophysical Research Letters*, 34, n/a–n/a, doi:10.1029/2007GL029475, <http://dx.doi.org/10.1029/2007GL029475>, 112706, 2007.

15 Petit, J.-R., Jouzel, J., Raynaud, D., Barkov, N. I., Barnola, J.-M., Basile, I., Bender, M., Chappellaz, J., Davis, M., Delaygue, G., et al.: Climate and atmospheric history of the past 420,000 years from the Vostok ice core, Antarctica, *Nature*, 399, 429–436, 1999.

PMIP3: Paleoclimate Modelling Intercomparison Project Phase III, <https://pmip3.lsce.ipsl.fr/>.

Quere, C. L., Harrison, S. P., Colin Prentice, I., Buitenhuis, E. T., Aumont, O., Bopp, L., Claustre, H., Cotrim Da Cunha, L., Geider, R., Giraud, X., et al.: Ecosystem dynamics based on plankton functional types for global ocean biogeochemistry models, *Global Change Biology*, 11, 2016–2040, 2005.

Raven, J., Caldeira, K., Elderfield, H., Hoegh-Guldberg, O., Liss, P., Riebesell, U., Shepherd, J., Turley, C., and Watson, A.: Ocean acidification due to increasing atmospheric carbon dioxide, *The Royal Society*, 2005.

Redfield, A. C.: The influence of organisms on the composition of sea-water, *The Sea*, 2, 26–77, 1963.

Ridgwell, A., Hargreaves, J. C., Edwards, N. R., Annan, J. D., Lenton, T. M., Marsh, R., Yool, A., and Watson, A.: Marine geochemical data assimilation in an efficient Earth System Model of global biogeochemical cycling, *Biogeosciences*, 4, 87–104, 2007.

Sarmiento, J. and Toggweiler, J.: A new model for the role of the oceans in determining atmospheric pCO<sub>2</sub>, *Nature*, 308, 621–624, 1984.

Sarmiento, J. L. and Gruber, N.: *Ocean biogeochemical dynamics*, Princeton University Press, 2006.

Schmittner, A., Green, J. A. M., and Wilmes, S.-B.: Glacial ocean overturning intensified by tidal mixing in a global circulation model, *Geophysical Research Letters*, 42, 4014–4022, 2015.

30 Sigman, D. M. and Boyle, E. A.: Glacial/interglacial variations in atmospheric carbon dioxide, *Nature*, 407, 859–869, 2000.

Sigman, D. M., Hain, M. P., and Haug, G. H.: The polar ocean and glacial cycles in atmospheric CO<sub>2</sub> concentration, *Nature*, 466, 47–55, 2010.

Sikes, E. L., Samson, C. R., Guilderson, T. P., and Howard, W. R.: Old radiocarbon ages in the southwest Pacific Ocean during the last glacial period and deglaciation, *Nature*, 405, 555–559, 2000.

35 Sime, L. C., Kohfeld, K. E., Le Quéré, C., Wolff, E. W., de Boer, A. M., Graham, R. M., and Bopp, L.: Southern Hemisphere westerly wind changes during the Last Glacial Maximum: model-data comparison, *Quaternary Science Reviews*, 64, 104–120, 2013.

Skinner, L., Fallon, S., Waelbroeck, C., Michel, E., and Barker, S.: Ventilation of the deep Southern Ocean and deglacial CO<sub>2</sub> rise, *Science*, 328, 1147–1151, 2010.



Skinner, L., McCave, I., Carter, L., Fallon, S., Scrivner, A., and Primeau, F.: Reduced ventilation and enhanced magnitude of the deep Pacific carbon pool during the last glacial period, *Earth and Planetary Science Letters*, 411, 45–52, 2015.

Takahashi, T., Broecker, W. S., and Langer, S.: Redfield ratio based on chemical data from isopycnal surfaces, *Journal of Geophysical Research: Oceans*, 90, 6907–6924, 1985.

5 Toggweiler, J. R., Gnanadesikan, A., Carson, S., Murnane, R., and Sarmiento, J. L.: Representation of the carbon cycle in box models and GCMs: 1. Solubility pump, *Global Biogeochemical Cycles*, 17, n/a–n/a, doi:10.1029/2001GB001401, <http://dx.doi.org/10.1029/2001GB001401>, 1026, 2003.

Volk, T. and Hoffert, M. I.: Ocean Carbon Pumps: Analysis of Relative Strengths and Efficiencies in Ocean-Driven Atmospheric CO<sub>2</sub> Changes, in: *The Carbon Cycle and Atmospheric CO<sub>2</sub>: Natural Variations Archean to Present*, edited by Sundquist, E. T. and Broecker, W. S., American Geophysical Union, Washington D.C., 1985.

10 Wanninkhof, R.: Relationship between gas exchange and wind speed over the ocean, *Journal of Geophysical Research*, 97, 7373–7382, 1992.

Williams, R. G. and Follows, M. J.: *Ocean Dynamics and the Carbon Cycle: Principles and Mechanisms*, Cambridge University Press, 2011.

Zeebe, R. E. and Wolf-Gladrow, D. A.: CO<sub>2</sub> in seawater: equilibrium, kinetics, isotopes, 65, Gulf Professional Publishing, 2001.

15 Zhang, X., Lohmann, G., Knorr, G., and Xu, X.: Different ocean states and transient characteristics in Last Glacial Maximum simulations and implications for deglaciation, *Climate of the Past*, 9, 2319–2333, doi:10.5194/cp-9-2319-2013, <http://www.clim-past.net/9/2319/2013/>, 2013.

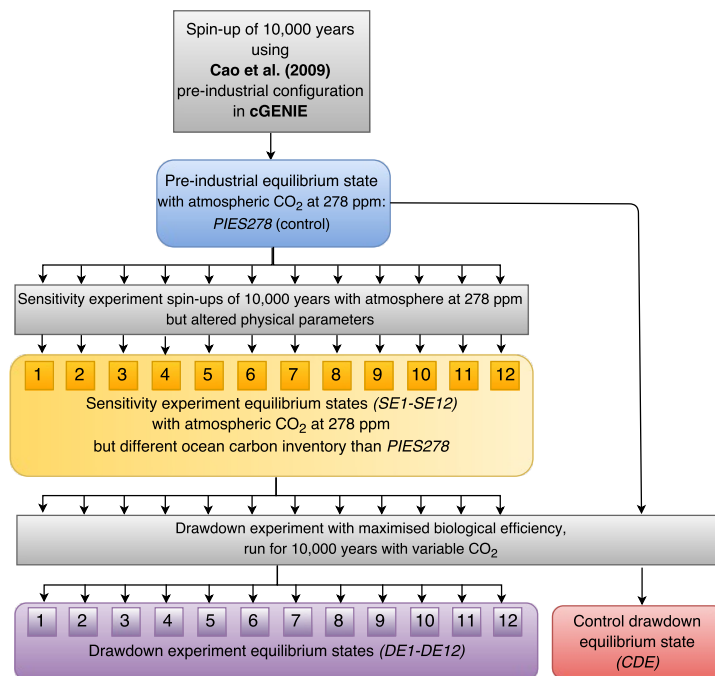


**Figure 1.** Flow chart showing the experimental setup. Grey boxes are spin-ups and transient stages of simulations (not analysed). Coloured boxes are equilibrium states that are analysed in this study. Throughout the study, the pre-industrial equilibrium state PIES278 (light blue box) is used as the control state, with which we compare the sensitivity experiment equilibrium states SE1–SE12 (yellow box). The change in physical characteristics for each SE state compared to the control state PIES278 is described in Table 1. The SE:s are then used as a basis for the CO<sub>2</sub> experiments where biological efficiency is maximised. After running the drawdown experiments for 10,000 model years, we achieve a new ensemble of drawdown equilibrium states (DE1 – DE12) which are compared to a control drawdown equilibrium state (CDE).

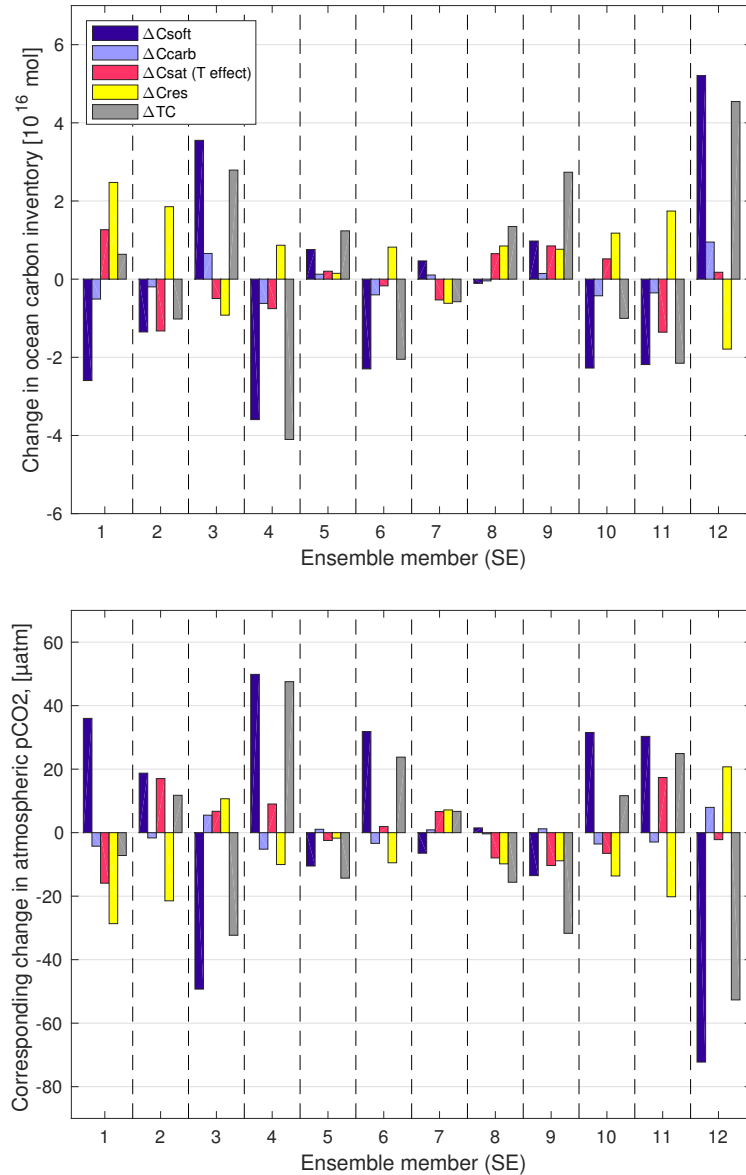


**Figure 2.** The upper panel shows observed  $\Delta TC$  (grey bars) for SE1 – SE12, as compared to the TC inventory of the control *PIES278*, and the relative contributions by changes in the biological soft tissue (dark blue bars), hard tissue (light purple bars) and solubility (red bars) pumps. The contribution to the change in the solubility pump by changes in preformed alkalinity is so small that it can not be seen in this type of diagram and is therefore excluded. Hence, only the contribution to  $C_{sat}$  by the change in temperature is shown. The residual of the theoretical contributions by changes in  $C_{soft}$ ,  $C_{carb}$  and  $C_{sat}$  to  $\Delta TC$  (calculations made using Eqs. (9)–(13)) and the observed model  $\Delta TC$  is denoted  $C_{res}$  (yellow bars). The left hand axis shows magnitude of changes given in  $10^{16}$  mol ( $\sim 120$  Pg C). The lower panel shows  $pCO_2^{atm}$  equivalent given in  $\mu\text{atm}$ . Hence, this shows how big the difference in  $pCO_2^{atm}$  would be between ensemble members if we were not restoring to 278 ppm. Note that a positive (negative)  $\Delta TC$  indicates a higher (lower) storage of CO<sub>2</sub> in the ocean, which would cause a lower (higher)  $pCO_2^{atm}$ .

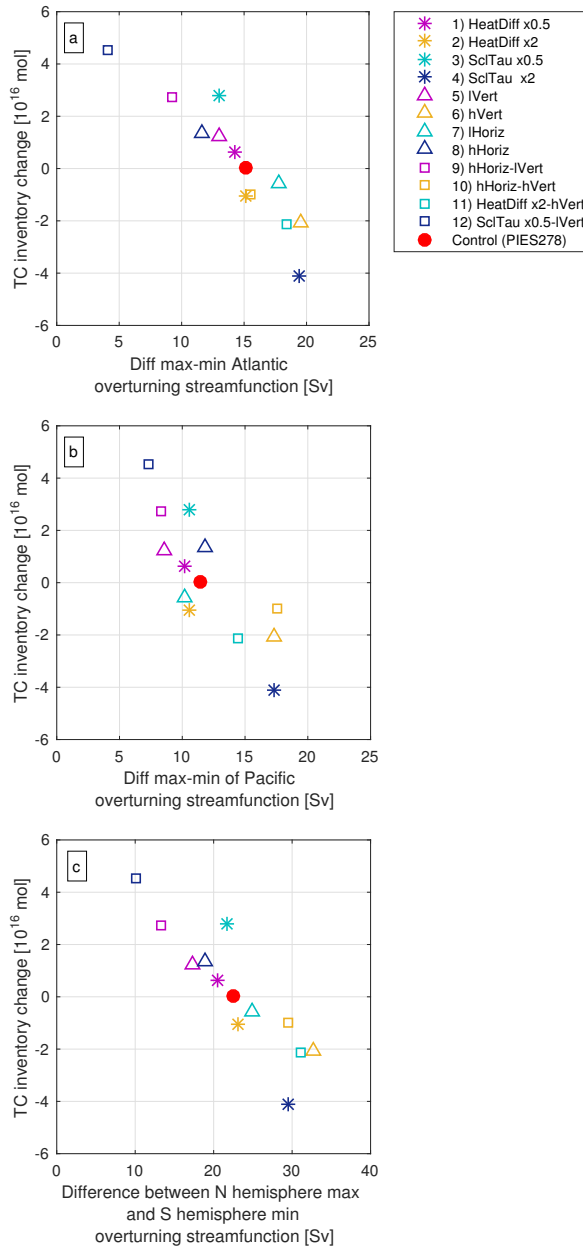


**Figure 3.** The difference between the maximum and minimum of the zonal average overturning streamfunction,  $\psi$ , below 556 m depth, and the change in  $TC$  for equilibrium states  $SE1 - SE12$  c.f. the control  $PIES278$  (red dot). This is shown for the Atlantic basin, Pacific basin and for a global measure based on hemispheric differences, on the horizontal axis of panels a, b and c respectively.

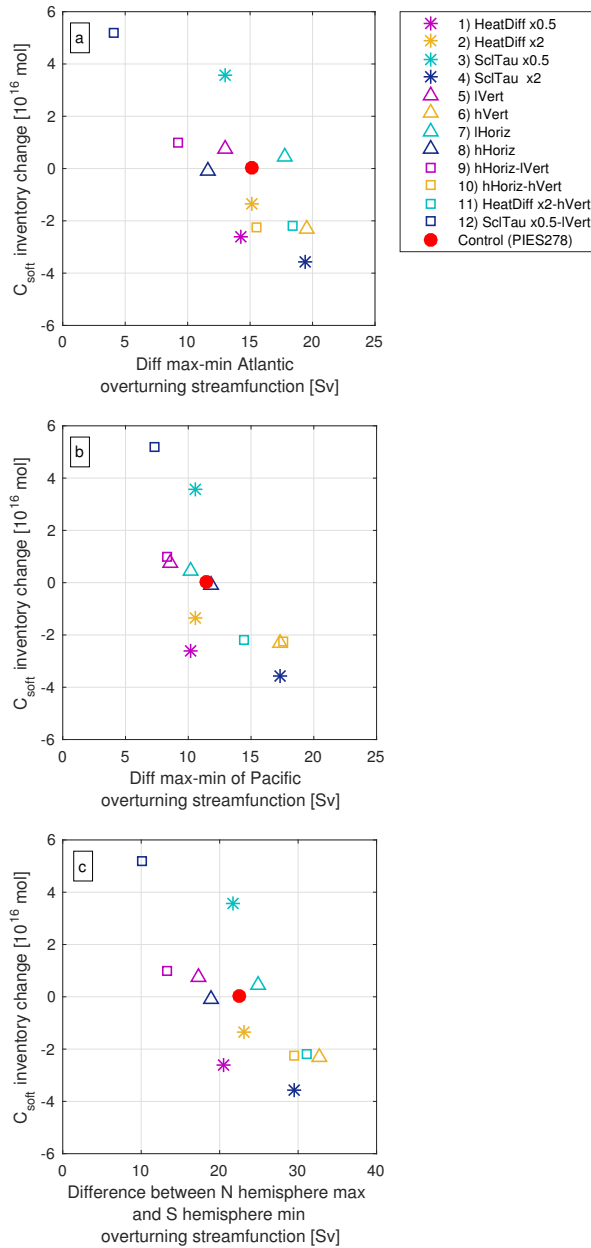


**Figure 4.** The difference between the maximum and minimum of the zonal average overturning streamfunction,  $\psi$ , below 556 m depth, and the change in  $C_{soft}$  for equilibrium states  $SE1 - SE12$  c.f. the control  $PIES278$  (red dot). This is shown for the Atlantic basin, Pacific basin and for a global measure based on hemispheric differences, on the horizontal axis of panels a, b and c respectively.

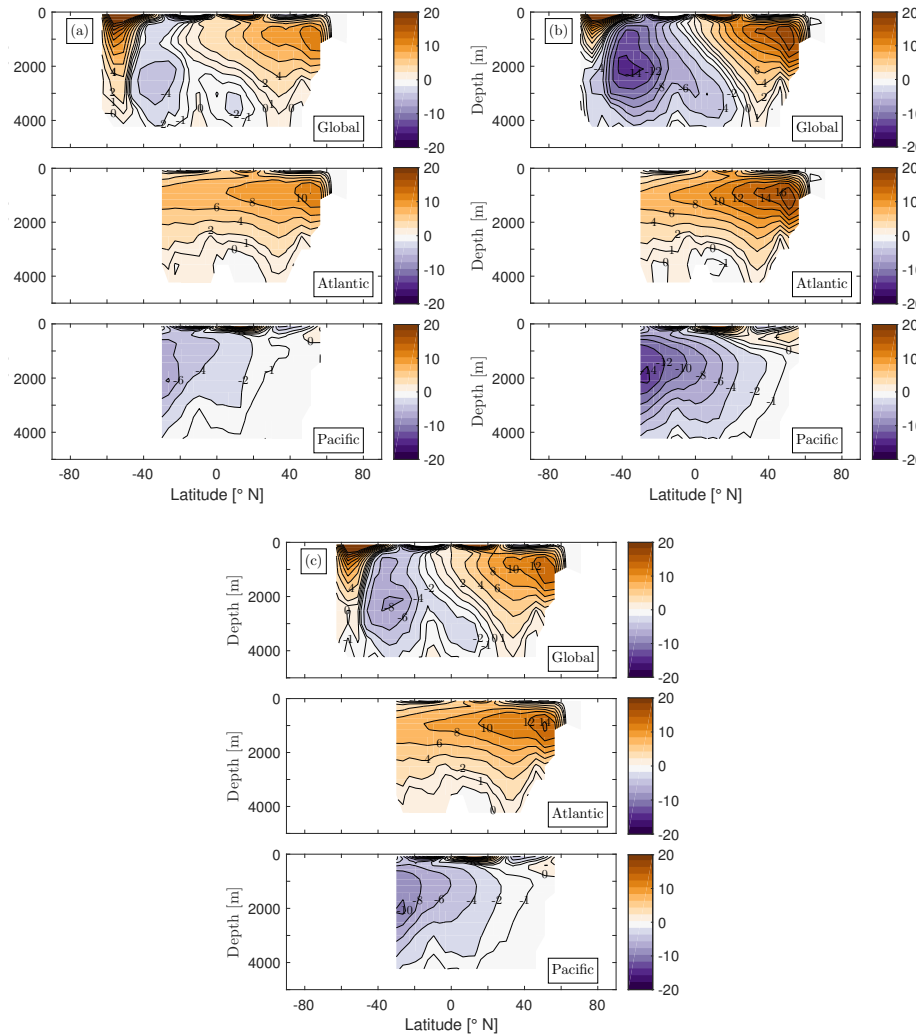


**Figure 5.** Zonal average overturning streamfunction ( $\psi$ ) in Sverdrup Sv for a) SE5, with low vertical diffusivity, b) SE6, with high vertical diffusivity and c) the control PIES278. The upper panel shows the global  $\psi$ , the middle panel shows only the Atlantic sector and the lower panel shows only the Pacific sector. The southernmost limit for the Atlantic and Pacific sectors is  $-30^{\circ}$  N.

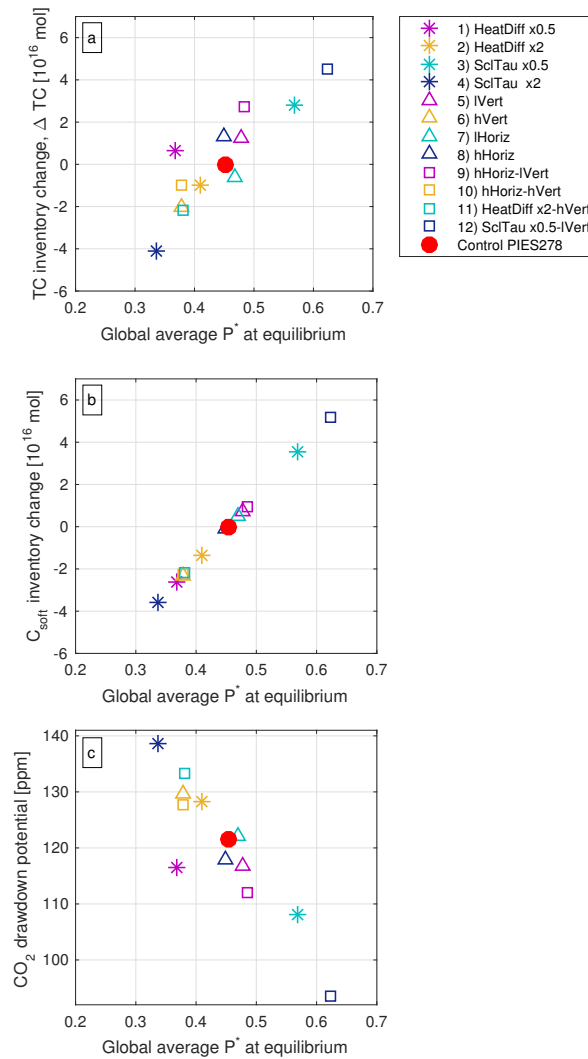


**Figure 6.** Panels showing (whole) global ocean  $\bar{P}^*$  for the different ensemble members  $SE1 - SE12$  plotted versus a)  $\Delta TC$  ( $10^{16}$  mol), b) the inventory change of  $C_{soft}$ , hence  $M_o \cdot \Delta C_{soft}$ , and c) the  $CO_2$  drawdown potential (ppm) of each ensemble member, which is the lowering of  $pCO_2^{atm}$  achieved by maximising biological efficiency (making  $\bar{P}^*$  get equal to 1), see Eq. (3). Ensemble member characteristics are described in Table 1.

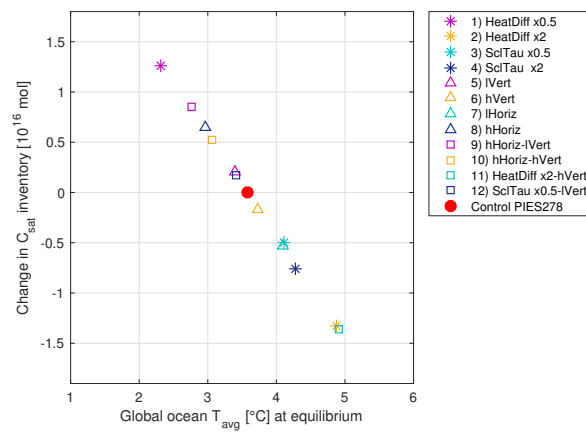


**Figure 7.** Global ocean average temperature ( $T_{avg}$ ) and the changes in  $C_{sat}$  for the ensemble members  $SE1 - SE12$  compared to the control simulation  $PIES278$  (red dot).

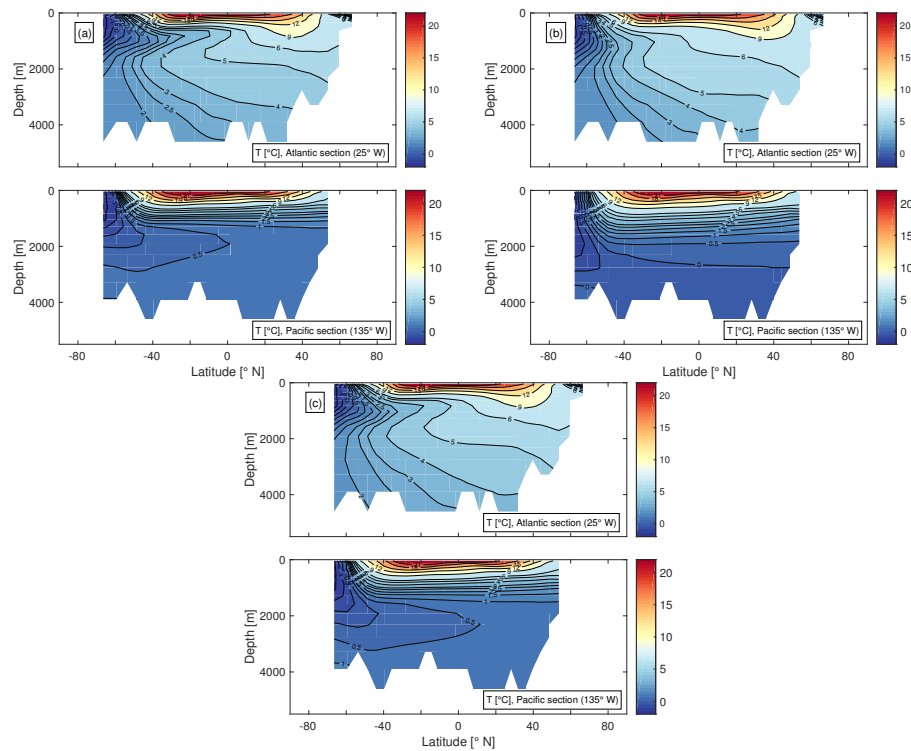


**Figure 8.** Sections of temperature ( $^{\circ}\text{C}$ ) for a) *SE5*, with low vertical diffusivity, b) *SE6*, with high vertical diffusivity and c) the control *PIES278*. The upper panel of each subfigure shows a section through the Atlantic, at  $25^{\circ}$  W and the lower panel shows a section through the Pacific, at  $135^{\circ}$  W. Both sections also cover latitudes that are in the Southern Ocean (south of  $-30^{\circ}$  N).

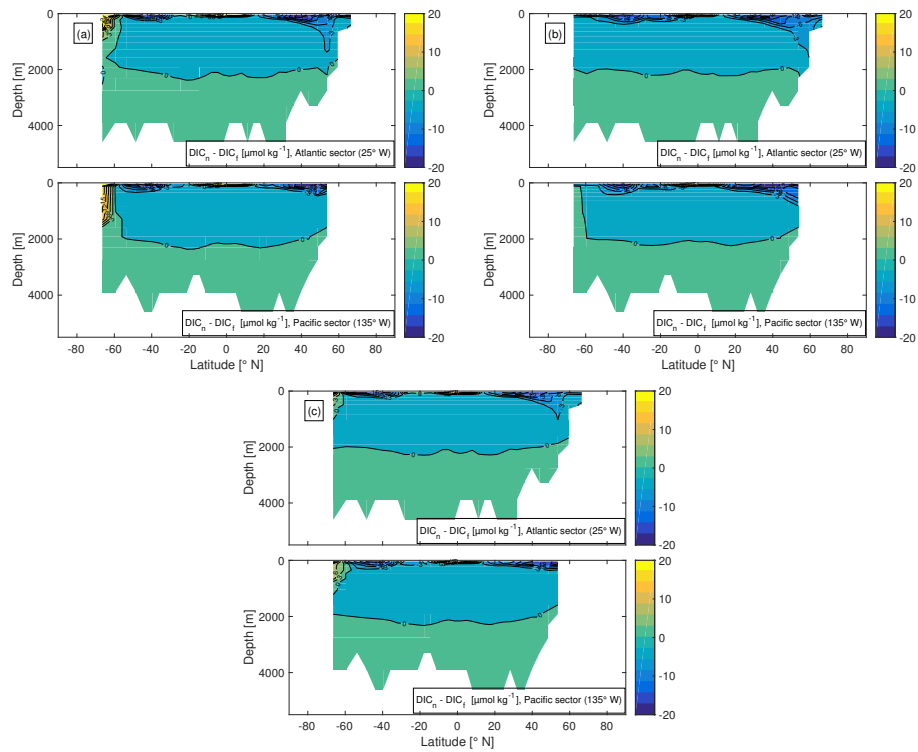


**Figure 9.** Example sections of the DIC concentration difference  $DIC_n - DIC_f$ , where  $DIC_n$  is the concentration in model simulations with normal gas exchange for  $CO_2$  and  $DIC_f$  is the concentration in model simulations with artificially fast gas exchange for  $CO_2$ . The panels show  $DIC_n - DIC_f$  for a) SE1, with halved atmospheric heat diffusivity, b) SE4, with doubled wind stress and c) the control equilibrium PIES278. The upper panel of each subfigure shows a section through the Atlantic, at  $25^\circ$  W and the lower panel shows a section through the Pacific, at  $135^\circ$  W. Both sections also cover latitudes that are in the Southern Ocean (south of  $-30^\circ$  N).

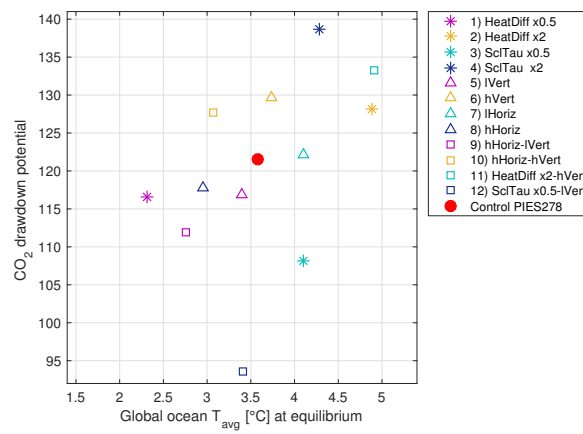


**Figure 10.** Global ocean average temperature ( $T_{avg}$ ,  $^{\circ}\text{C}$ ) in relation to drawdown potential for  $\text{CO}_2$  ( $DP$ , ppm) for all ensemble members  $SE1 - SE12$  and the control  $PIES278$  (red dot).



**Table 1.** List of sensitivity experiment equilibrium states  $SE1 - SE12$ , abbreviated ensemble member description, and specification of which one or two physical characteristics have been altered compared to the control  $PIES278$ . The nature of the change is specified within parenthesis.

Ensemble member	Abbreviated description	Adjusted parameter (adjustment)
SE1	'HeatDiff x0.5'	Atmospheric heat diffusivity (halved)
SE2	'HeatDiff x2'	Atmospheric heat diffusivity (doubled)
SE3	'SciTau x0.5'	Wind stress intensity (halved)
SE4	'SciTau x2'	Wind stress intensity (doubled)
SE5	'lVert'	Ocean vertical diffusivity (halved)
SE6	'hVert'	Ocean vertical diffusivity (doubled)
SE7	'lHoriz'	Ocean horizontal diffusivity (halved)
SE8	'hHoriz'	Ocean horizontal diffusivity (doubled)
SE9	'hHoriz-lVert'	Ocean horizontal, and vertical diffusivity (doubled, halved)
SE10	'hHoriz-hVert'	Ocean horizontal, and vertical diffusivity (doubled, doubled)
SE11	'HeatDiff x2 hVert'	Atmospheric heat diffusivity (doubled) and ocean vertical diffusivity (doubled)
SE12	'SciTau x0.5 lVert'	Wind stress intensity (halved) and ocean vertical diffusivity (halved)



**Table 2.** Diagnostic variables for observations (Obs.), the control *PIES278* (Ctrl.) and the ensemble members *SE1* – *SE12*. The variables are global ocean averages of temperature ( $T_{avg}$ , °C) and  $pH$  ( $pH_{avg}$ ), surface ocean average  $pH$ , the sea ice cover (%), the global average of the nutrient utilisation efficiency (expressed in terms of  $\overline{P^*}$ ) and a measure of the strength of the global ocean overturning circulation,  $\psi$ , which is the difference between the Northern hemisphere maximum and the Southern hemisphere minimum (1 Sv =  $1 \cdot 10^6 \text{ m}^3 \text{ s}^{-1}$ ) below 556 m. Observational estimate for  $T_{avg}$  has been calculated using World Ocean Atlas 2013, Locarnini et al. (2013)) and the pre-industrial estimate for  $pH$  is given by Raven et al. (2005). Modern day sea ice cover is given as an interval due to seasonal variability Comiso (2008). The observational estimate for  $\overline{P^*}$  is given by Ito and Follows (2005)

Ens. mem.	$T_{avg}$ (°C)	$pH_{avg}$ (SWS)	$pH_{surf}$ (SWS)	Sea ice cover (%)	Global $\overline{P^*}$	Global $\psi_{max} - \psi_{min}$ (Sv)
Obs.	3.49	-	~8.2	3 to 6	0.36	–
Ctrl.	3.58	7.90	8.16	5.4	0.45	22.5
SE1	2.31	7.89	8.15	10.6	0.37	20.6
SE2	4.88	7.91	8.17	0.7	0.41	23.2
SE3	4.10	7.84	8.16	6.7	0.57	21.6
SE4	4.28	7.97	8.16	2.7	0.34	29.4
SE5	3.39	7.87	8.15	6.1	0.48	17.4
SE6	3.73	7.94	8.16	4.1	0.38	32.6
SE7	4.10	7.90	8.16	5.3	0.47	24.8
SE8	2.96	7.88	8.16	5.4	0.45	19.0
SE9	2.76	7.85	8.15	6.0	0.48	13.4
SE10	3.07	7.93	8.16	3.7	0.38	30.0
SE11	4.91	7.93	8.17	0.0	0.38	31.1
SE12	3.41	7.80	8.15	7.4	0.62	10.1



**Table 3.** Correlation coefficients of the changes in strength of the zonal average overturning streamfunction ( $\psi_{max} - \psi_{min}$ ) below 556 m depth in different geographical regions and the changes in carbon species. Global means the difference between the Northern Hemisphere maximum and the Southern Hemisphere minimum overturning.

$(\psi_{max} - \psi_{min})$ in region	$\Delta TC$	$\Delta C_{sat}$ (T effect)	$\Delta C_{soft}$	$\Delta C_{res}$	$\Delta C_{soft}$ $+\Delta C_{res}$
Atlantic	-0.924	-0.485	-0.793	0.476	-0.871
Pacific	-0.810	-0.256	-0.733	0.402	-0.832
Global	-0.893	-0.488	-0.756	0.445	-0.836